iScience

CellPress

Article

Marked Global DNA Hypomethylation Is Associated with Constitutive PD-L1 Expression in Melanoma

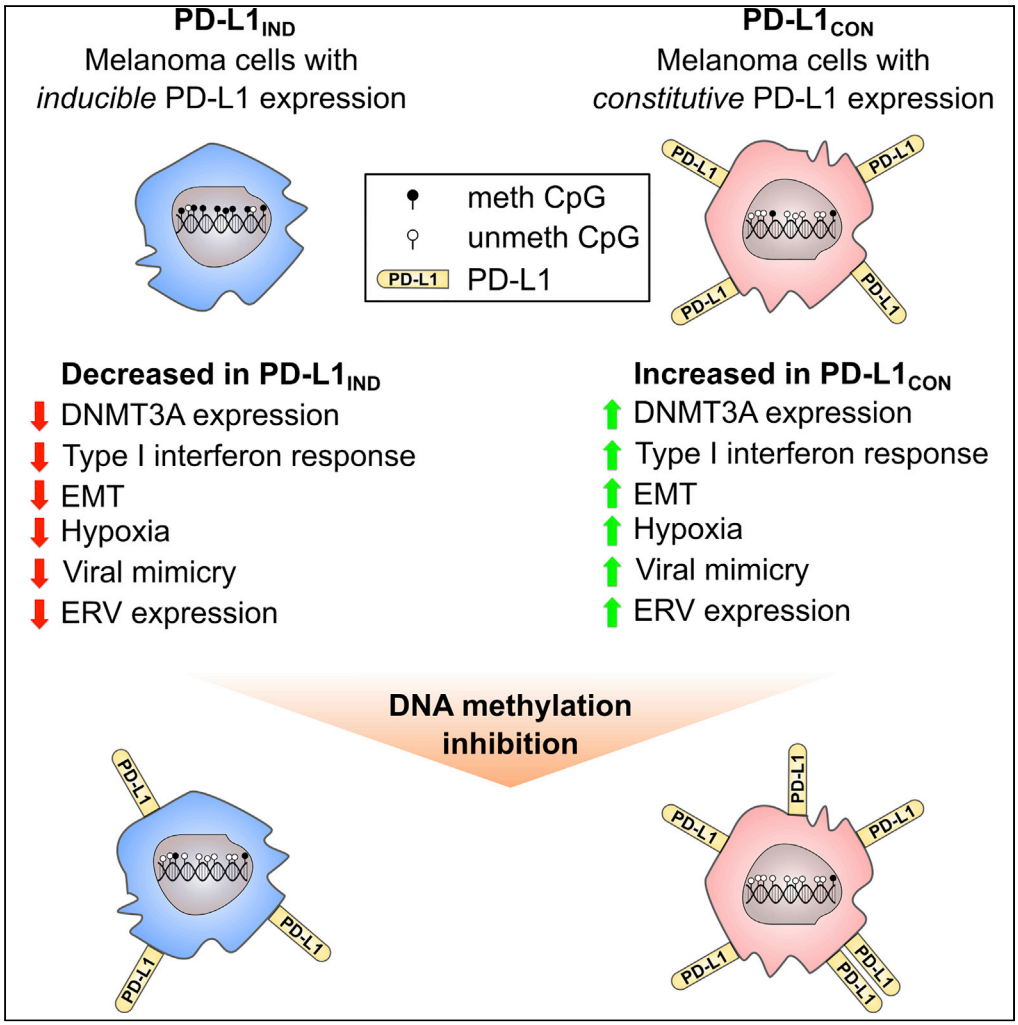

Aniruddha Chatterjee, Euan J. Rodger, Antonio Ahn, ..., Jessamy Tiffen, Michael R. Eccles, Peter Hersey

aniruddha.chatterjee@otago.ac.nz (A.C.)
michael.eccles@otago.ac.nz (M.R.E.)
p.hersey@centenary.org.au (P.H.)

HIGHLIGHTS

Global DNA hypomethylation in melanoma promotes constitutive PD-L1 expression

Transcriptomic up-regulation accompanies constitutive PD-L1 expression in melanoma

Constitutive PD-L1 is associated with reduced *DNMT3A* expression and viral mimicry

DNA methylation inhibitor treatment of melanoma cells increases PD-L1 expression

DATA AND SOFTWARE AVAILABILITY

GSE107622

Chatterjee et al., iScience 4, 312–325
June 29, 2018
https://doi.org/10.1016/j.isci.2018.05.021

iScience

CellPress

Article

Marked Global DNA Hypomethylation Is Associated with Constitutive PD-L1 Expression in Melanoma

Aniruddha Chatterjee,[1,2,5,*] Euan J. Rodger,[1,2,5] Antonio Ahn,[1] Peter A. Stockwell,[1] Matthew Parry,[3] Jyoti Motwani,[1] Stuart J. Gallagher,[4] Elena Shklovskaya,[4] Jessamy Tiffen,[4] Michael R. Eccles,[1,2,6,7,*] and Peter Hersey[4,6,*]

SUMMARY

Constitutive expression of the immune checkpoint, PD-L1, inhibits anti-tumor immune responses in cancer, although the factors involved in PD-L1 regulation are poorly understood. Here we show that loss of global DNA methylation, particularly in intergenic regions and repeat elements, is associated with constitutive ($PD\text{-}L1_{CON}$), versus inducible ($PD\text{-}L1_{IND}$), PD-L1 expression in melanoma cell lines. We further show this is accompanied by transcriptomic up-regulation. *De novo* epigenetic regulators (e.g., *DNMT3A*) are strongly correlated with PD-L1 expression and methylome status. Accordingly, decitabine-mediated inhibition of global methylation in melanoma cells leads to increased PD-L1 expression. Moreover, viral mimicry and immune response genes are highly expressed in lymphocyte-negative plus PD-L1-positive melanomas, versus PD-L1-negative melanomas in The Cancer Genome Atlas (TCGA). In summary, using integrated genomic analysis we identified that global DNA methylation influences PD-L1 expression in melanoma, and hence melanoma's ability to evade anti-tumor immune responses. These results have implications for combining epigenetic therapy with immunotherapy.

INTRODUCTION

Immunotherapy with monoclonal antibodies (mAbs) that block PD-1/PD-L1 interactions on immune cells has shown remarkable success in the treatment of melanoma (Hersey and Gowrishankar, 2015; Hodi et al., 2016; Ribas et al., 2016; Ugurel et al., 2016) and other malignancies (Gandini et al., 2016; Ansell et al., 2015). PD-1 (*CD279*) is an inhibitory molecule that inhibits T-cell receptor (TCR) signaling on T cells by increasing the threshold necessary for their activation and effector function. As such, it is often expressed on activated CD4 and CD8 T cells, but other immune cells (e.g., NK and B cells and monocytes) may also express this molecule. PD-1 engages primarily with its ligands PD-L1 (B7-H1, *CD274*) and PD-L2 (B7-DC, *CD273*) (Greenwald et al., 2005; Yao et al., 2013), which are widely expressed not only on immunocompetent cells but also in non-lymphoid organs (Dong et al., 2004; Greenwald et al., 2005).

Melanoma cells commonly express PD-L1 as an adaptive response to T cell recognition (Gowrishankar et al., 2015; Ribas, 2015). This results in activation of the inhibitory PD-1 receptor on T cells that infiltrate the tumor microenvironment, resulting in inhibition of their activity (Schildberg et al., 2016) and allowing melanoma cells to evade the host immune system. Up-regulation of PD-L1 on melanoma cells is believed to result from interferon gamma (IFN-γ) release by T cells that interact with the tumor. IFN-γ then signals through the type II IFN receptor by activating the JAK/STAT pathway. STAT then interacts in the nucleus with IFN-γ activation sites (GAS) in the promoters of IFN-stimulated genes (Platanias, 2005).

A number of studies have examined whether PD-L1 may be a biomarker to help select responders to anti-PD-1 inhibitors, but as a single marker it has been of limited value mainly because of its variable expression (Madore et al., 2014) and the detection of responses in patients with PD-L1-negative tumors (Daud et al., 2016; Festino et al., 2016). We (Madore et al., 2014) and others (Smyth et al., 2016; Taube et al., 2012; Topalian et al., 2016) have shown that patients can be subdivided into at least four groups depending on the expression of PD-L1 and T lymphocyte infiltration (TIL). In a large proportion of patients (approximately 30%) PD-L1 expression is associated with infiltration of the tumor by TILs (TIL+/PD-L1+). In 20% there are TILs but no PD-L1 expression (TIL+/PD-L1−), and in 40% there are neither TILs nor PD-L1 expression (TIL−/PD-L1−) (Ribas, 2015; Topalian et al., 2016). The remaining melanomas exhibit diffuse expression

[1]Department of Pathology, Dunedin School of Medicine, University of Otago, 270 Great King Street, Dunedin 9054, New Zealand

[2]Maurice Wilkins Centre for Molecular Biodiscovery, Level 2, 3A Symonds Street, Auckland, New Zealand

[3]Department of Mathematics & Statistics, University of Otago, 710 Cumberland Street, Dunedin 9054, New Zealand

[4]Melanoma Immunology and Oncology Group, The Centenary Institute, University of Sydney, Royal Prince Alfred Hospital, Missenden Road, Camperdown, NSW 2050, Australia

[5]These authors contributed equally

[6]Senior author

[7]Lead Contact

*Correspondence: aniruddha.chatterjee@otago.ac.nz (A.C.), michael.eccles@otago.ac.nz (M.R.E.), p.hersey@centenary.org.au (P.H.)

https://doi.org/10.1016/j.isci.2018.05.021

of PD-L1 without the presence of TILs (TIL−/PD-L1+), which is referred to as constitutive PD-L1 expression. Previous authors have speculated that constitutive expression is due to oncogene-driven expression (Pardoll, 2012), but we (Gowrishankar et al., 2015) and others have excluded a number of potential oncogenic pathways that have been implicated in other cancers (Spranger and Gajewski, 2016).

To better understand the basis for constitutive expression of PD-L1 we have examined whether epigenetic mechanisms play a potential role in the regulation of PD-L1 expression. Previous studies in non-small cell lung cancer cell lines have shown up-regulation of PD-L1 after treatment with the demethylating agent azacytidine (Wrangle et al., 2013). Similar findings were reported in studies on breast, colon, and ovarian carcinoma lines (Li et al., 2014). Additional evidence that DNA methylation may constitute an additional regulatory mechanism came from Madore et al. (2016) who found that low or absent PD-L1 expression in 52 patients with melanoma in The Cancer Genome Atlas (TCGA) was associated with high levels of DNA methylation, as assessed using Illumina 450K arrays. In view of these findings, we have explored whether epigenetic mechanisms associated with DNA methylation could underlie the constitutive expression of PD-L1 on melanoma, by either silencing repressive factors or by activation of pathways that normally regulate PD-L1 expression.

RESULTS

Characterization of Inducible and Constitutive Patterns of Expression of PD-L1 (PD-L1$_{IND}$ and PD-L1$_{CON}$) in Melanoma Cell Lines

To characterize the expression patterns of PD-L1 in melanoma, we investigated cell surface PD-L1 expression in melanoma cell lines and selected six cell lines that constitutively expressed PD-L1 (PD-L1 positive, referred to as PD-L1$_{CON}$) and six cell lines that expressed PD-L1 only upon induction after treatment with IFN-γ (PD-L1 negative, referred to as PD-L1$_{IND}$) (Figure 1). The percentage of PD-L1-positive cells in PD-L1$_{CON}$ cell lines ranged from 41.6% to 99.07% (median = 93.57%), whereas the proportion of PD-L1-positive cells in PD-L1$_{IND}$ was confirmed to be very low (0.82%–6.79% [median = 1.7%, Figure 1, details in Table S1 and Figures S1 and S2]). Some PD-L1$_{CON}$ cell lines constitutively produced significant amounts of IFN-γ (Gallagher et al., 2014), and therefore we considered the possibility of a role for IFN-γ feedback in maintaining the constitutive PD-L1 expression on these cells. However, blockade of interferon type I or type II signaling did not affect constitutive PD-L1 expression in two PD-L1$_{CON}$ cell lines (Figure S3). Furthermore, the presence of common oncogenic driver mutations was similar between each group of cell lines; each group contained four cell lines harboring a *BRAFV600E* mutation, one with a *NRASQ61* mutation and one wild-type for *NRAS* and *BRAF* (Table S1). These data suggest that factors other than IFN-γ, or oncogenic signaling, are involved in regulating PD-L1 expression.

Whole-Genome-Scale DNA Methylation Identifies Extensive Global Hypomethylation in Constitutive PD-L1 Cell Lines (PD-L1$_{CON}$)

We generated genome-scale DNA methylation maps by performing reduced representation bisulfite sequencing (RRBS) (Chatterjee et al., 2017b; Meissner et al., 2008) on the PD-L1$_{IND}$ and PD-L1$_{CON}$ lines. In total, we obtained 535 million sequence reads for the 12 cell lines, allowing the investigation of 290,385 MspI fragments consisting of 1.66 million reads at a high coverage (Chatterjee et al., 2017a) (Table S2). The striking finding from this analysis was that global genomic methylation levels in the PD-L1$_{CON}$ cell lines were much lower than those in PD-L1$_{IND}$ cell lines (median methylation = 0.47 and 0.63, respectively, Wilcoxon rank test p value $<2.2 \times 10^{-16}$, Figure 2 and Table S3). The hypomethylation of PD-L1$_{CON}$ cell lines was particularly pronounced in intergenic regions and in gene introns (Figure 2A). Intergenic regions showed a 19% median methylation reduction in PD-L1$_{CON}$, whereas for introns the median loss of methylation was 12%. Gene promoters (defined as −5 kb to +1 kb) were hypomethylated in both groups, and exon regions showed similar levels of methylation in both groups (Figure 2A and Table S3).

PD-L1$_{CON}$ cells showed hypomethylation in every class of repeat element analyzed (Figures 2B–2E and Table S4). Although hypomethylation was consistent in all repeat regions, the degree of methylation loss varied between subfamilies of repeats and individual elements. The LTR family showed the highest degree of hypomethylation in PD-L1$_{CON}$ compared with PD-L1$_{IND}$ cells (Figure 2E). For LTRs, the loss of median methylation ranged from 13% to 19%, with ERV1 showing the most significant hypomethylation. For LINE elements, the evolutionarily younger L1 showed a higher degree of hypomethylation (median methylation = 0.72 and 0.53 in PD-L1$_{IND}$ and PD-L1$_{CON}$, respectively, Figure 2B) than the evolutionarily older L2 element (median methylation 0.75 and 0.64 in PD-L1$_{IND}$ and PD-L1$_{CON}$ lines, respectively).

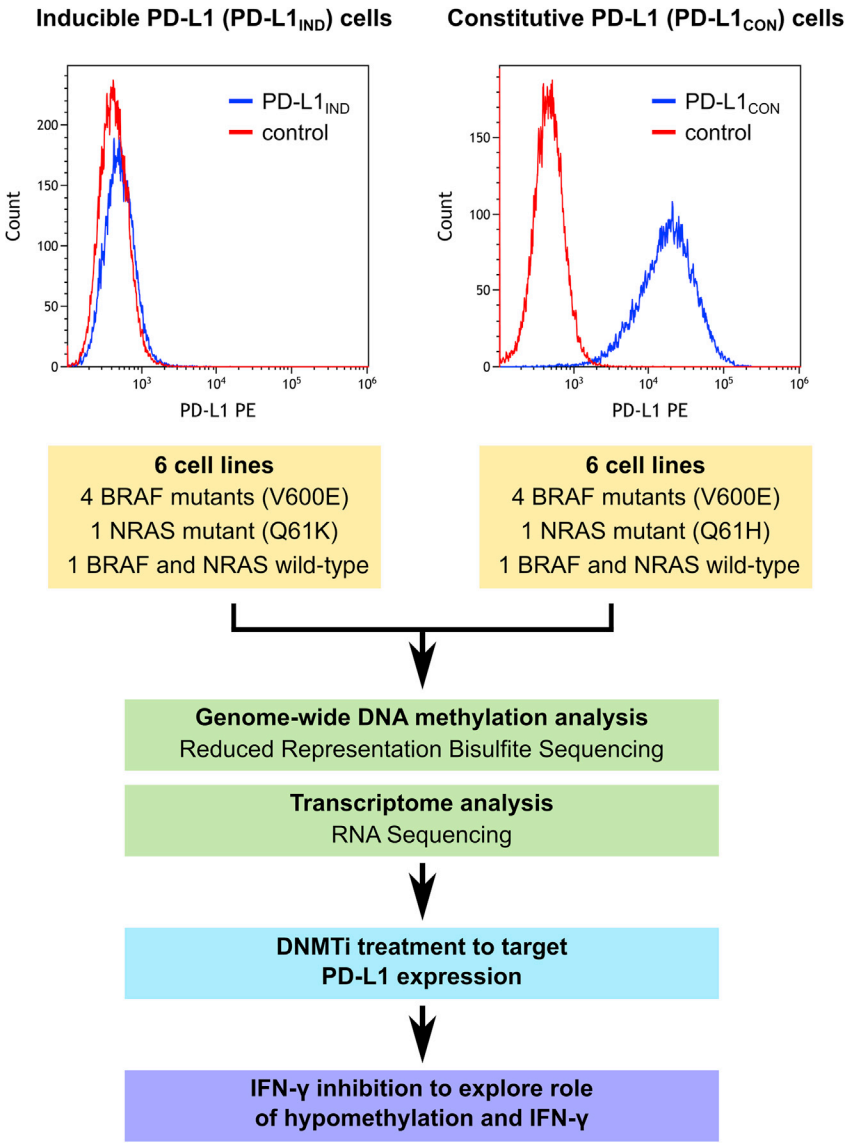

Figure 1. Summary of Experimental Design and the Analysis Pipeline for PD-L1$_{IND}$ and PD-L1$_{CON}$ Cell Lines to Identify Epigenetic Regulation of PD-L1 in Melanoma

Figure360▷ For a Figure360 author presentation of Figure 1, see http//dx.doi:10.1016/j.isci.2018.05.021#mmc3.

The upper panel shows representative FACS figures from PD-L1$_{CON}$ and PD-L1$_{IND}$ cells. See also Figures S1–S3, and Table S1.

Next, we identified 1,180 differentially methylated fragments (DMFs, F test at 5% false discovery rate (FDR) with 25% mean methylation difference for a fragment) that were mostly hypomethylated (96.4% of the DMFs) in PD-L1$_{CON}$ cell lines, consistent with the global patterns. There was a large difference in methylation levels (>50%) in three-quarters of the DMFs (Figures S4 and S5), and we identified 105 regions that showed >75% methylation differences between the PD-L1$_{IND}$ and PD-L1$_{CON}$ groups (Figure 2F). The strikingly divergent methylation pattern between the inducible and constitutive lines suggests there may be a common methylation-associated regulatory mechanism between the two groups.

To compare the RRBS methylation profiles observed in PD-L1$_{CON}$ and PD-L1$_{IND}$ cell lines with that of melanoma tumors, we analyzed 450K DNA methylation data from the TCGA-SKCM cohort. We specifically analyzed tumors that were TIL− to reduce the impact of immune cell signaling on tumor PD-L1 expression,

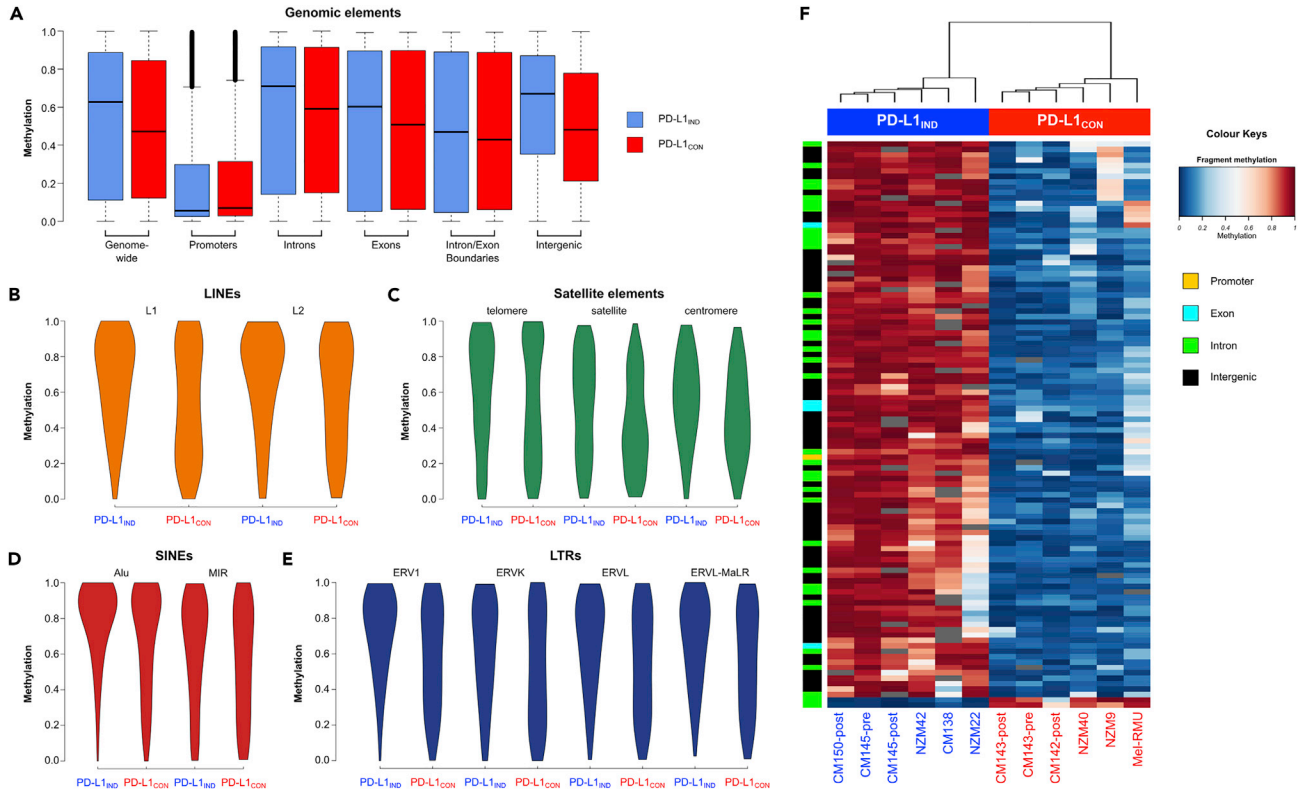

Figure 2. Whole-Genome-Scale and Element-Wise Methylation Profiles in PD-L1$_{IND}$ and PD-L1$_{CON}$ Cell Lines

(A) Boxplots showing genome-wide and genomic element RRBS methylation profiles for PD-L1$_{IND}$ (blue) and PD-L1$_{CON}$ (red) cell lines; black bars indicate the median methylation.

(B–E) Equal-area violin plots of PD-L1$_{CON}$ and PD-L1$_{IND}$ DNA methylation levels for different classes of repeat elements. (B) LINE elements (L1 and L2), (C) Satellite elements (satellite, telomeric, and centromeric repeats), (D) SINE elements (Alu and MIR), and (E) LTRs (ERV1, ERVK, ERVL, and ERVL-MaLR). In all cases the y axis represents the methylation level on a 0–1 scale. Annotations for repeat elements were downloaded from the UCSC repeat masker database.

(F) Methylation levels for the 105 differentially methylated fragments (DMFs) showing >70% methylation difference between the PD-L1$_{IND}$ and PD-L1$_{CON}$ cell lines (blue = unmethylated, red = fully methylated).

See also Figures S4–S9 and Tables S2–S4. The methylation data are available at Database: NCBI GEO, accession number GSE107622.

and we divided these tumors into group 1 (PD-L1−, n = 180) and group 2 (PD-L1+, n = 54). We considered these two groups as being the most representative of our analyzed inducible (group 1) and constitutive cell lines (group 2, Figures S6 and S7). We could not detect a significant global methylation difference between group 1 and group 2 melanomas (Figure S8), which we surmise is because of the promoter-biased design of the 450K probes and which suggests that RRBS has better discrimination power than the 450K platform to detect methylation differences in intergenic regions, introns, and repeat elements of melanomas. In addition, we specifically examined the five CpG island-associated probes in the promoter and 5′ untranslated region (5′UTR) of the gene for PD-L1 (*CD274*) in TCGA data. CpG probes cg02823866 and cg14305799 were located within 200 bp of the transcription start site (TSS) in the *CD274* promoter, whereas cg15837913 was located within 1,500 bp from the TSS and cg13474877 together with cg19724470 were within the *CD274* 5′UTR. The two CpGs in the *CD274* promoter were essentially unmethylated (<5% mean methylation) in both melanoma groups, whereas the two CpGs in the 5′UTR showed a loss of methylation (13% for cg15837913 and 16% for cg19724470) in group 2 (representative of constitutive melanoma) compared with group 1 (inducible melanoma, Figures S9A–S9E). These results are consistent with our RRBS data. We also analyzed the correlation of methylation in these probes with mRNA expression in the same patient groups and found the 5′UTR-associated cg19724470 methylation was significantly negatively correlated with PD-L1 expression (r = 0.49, p value = 1.44×10^{-15}, Figures S9F–S9J). These observations allude to the possibility that epigenetic modification of a distal enhancer or other distant elements might be involved in the regulation of *CD274* gene expression and identifying these elements would consequently be required for a full understanding of the overall regulatory processes controlling *CD274* gene expression.

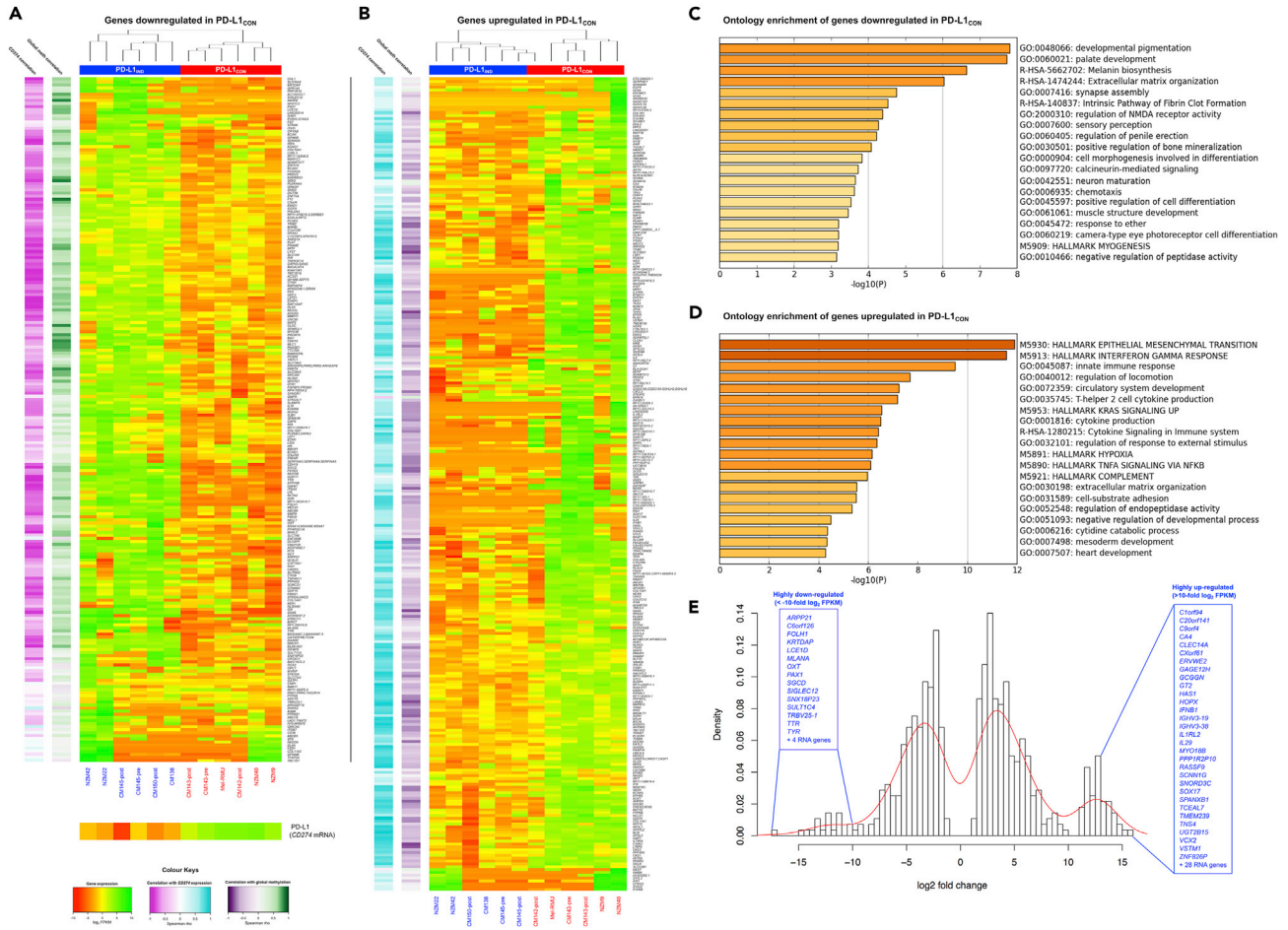

Figure 3. Differential Expression Patterns in PD-L1$_{IND}$ and PD-L1$_{CON}$ Cell Lines

(A) Mean-centered heatmap of the expression level (log_2 FPKMs) of 222 significantly down-regulated genes in PD-L1$_{CON}$.

(B) Mean-centered heatmap of the expression level (log_2 FPKMs) of 286 significantly up-regulated genes in PD-L1$_{CON}$. The correlations of these genes with *CD274* (PD-L1) expression and global methylation status in the analyzed cell lines are shown in the colored sidebars (left) in both figures.

(C) Enriched gene ontology terms relative to the 222 genes down-regulated in PD-L1$_{CON}$ cell lines.

(D) Enriched gene ontology terms relative to the 286 genes up-regulated in PD-L1$_{CON}$ cell lines. In figure (C) and (D), the x axis represents $-log_{10}$ of the p value.

(E) Density histogram of the log_2 fold changes for the significantly up-regulated (n = 286, right side of the histogram) and down-regulated (n = 222, left side of the histogram) genes. Genes with log_2 fold change >10 are indicated.

See also Figures S10–S12. The RNA-Seq data are available at Database: NCBI GEO, accession number GSE107622.

However, the impact of this difference in the methylation of a single CpG in the 5′UTR on the overall expression of *CD274* presently remains unclear. Nevertheless, we found that, overall, there was an insignificant difference in methylation of the *CD274* core promoter between the two groups.

Transcriptomic Features Reveal Distinct Differences in Expression Patterns between Constitutive and Inducible PD-L1 Lines

RNA sequencing (RNA-seq) analysis of the 12 cell lines identified 508 genes that were significantly differentially expressed (DEG) between PD-L1$_{IND}$ and PD-L1$_{CON}$ cell lines (p value <0.05, FDR corrected and log_2 fold change of mean FPKM $\geq$2). Of these DEGs, 222 genes were down-regulated (Figure 3A), whereas the remaining 286 genes were up-regulated in PD-L1$_{CON}$ cells (Figure 3B). Down-regulated genes in PD-L1$_{CON}$ lines were negatively correlated with *CD274* mRNA levels, for which expression was generally higher in PD-L1$_{CON}$ than PD-L1$_{IND}$ cell lines (see the bottom panel of Figure 3A), whereas up-regulated genes were positively correlated with *CD274* mRNA levels. This result suggests that the DEG profile in these cell lines could have a functional role in determining PD-L1 expression status. Up-regulated genes in

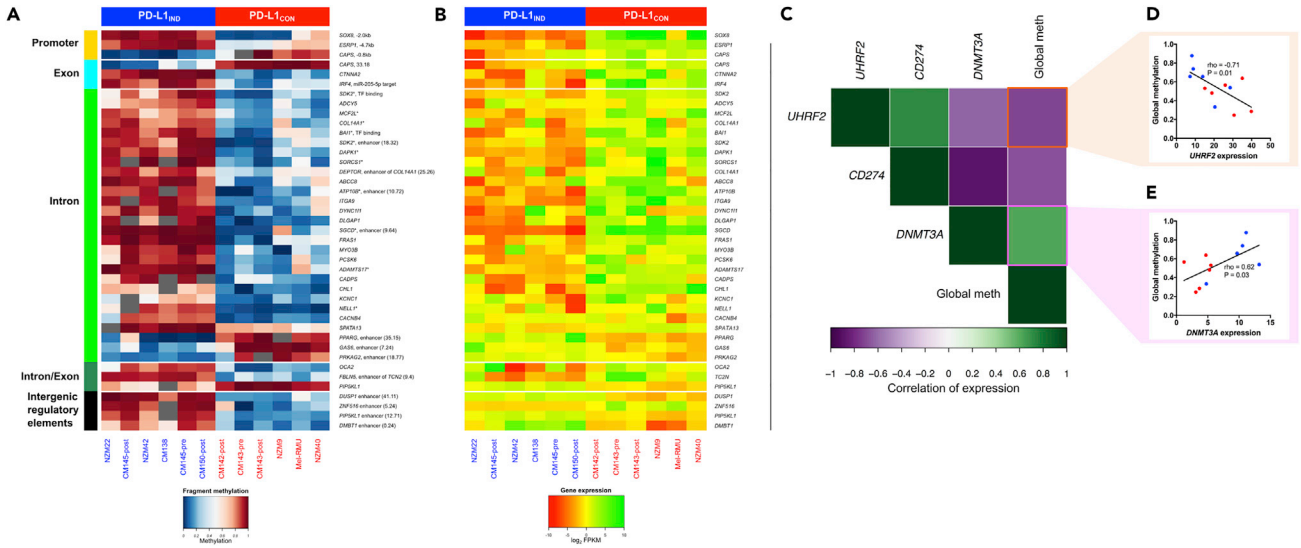

Figure 4. Differential Methylation Pattern and Relationship with Differential Expression in PD-L1$_{IND}$ and PD-L1$_{CON}$ Cell Lines and Role of Epigenetic Regulators

(A) Methylation heatmap of PD-L1$_{CON}$ and PD-L1$_{IND}$ cell lines for the differentially methylated fragments (DMFs) in different genomic elements showing the relationship with differential mRNA expression (blue = unmethylated, red = fully methylated). For several genes, multiple DMFs showed a strong correlation and are indicated as *.

(B) Mean-centered heatmap of the expression level (log_2 FPKMs) of the 39 genes that are regulated by methylation levels.

(C) Correlogram showing cross-correlation of the key epigenetic regulator genes with *CD274* (PD-L1) expression and global RRBS methylome levels.

(D and E) Relationship between mRNA level and RRBS methylome for the analyzed cell lines for *de novo* methylation machinery genes *UHRF2* (D) and *DNMT3A* (E). Spearman rho and statistical significance are shown.

See also Figures S13–S15 and Table S5.

PD-L1$_{CON}$ cell lines were strongly negatively correlated with global methylation levels, whereas down-regulated genes were positively correlated. We identified a group of 58 genes that showed very high up-regulation in PD-L1$_{CON}$ cell lines (log_2 fold change >10, Figure 3E, right side of the distribution) compared with 19 genes that showed very strong down-regulation in the PD-L1$_{CON}$ cell lines (Figure 3E, left distribution). The hypomethylated state of the PD-L1$_{CON}$ lines was possibly associated with the up-regulation of global mRNA expression in DEGs, which is conceptually similar to the up-regulation of gene expression upon reduction of DNA methylation levels following DNA methyl transferase (DNMT) inhibitor treatment (DNMTi), as reported in breast, ovarian, and colorectal cancer cell lines (Li et al., 2014).

Functional gene enrichment analysis revealed that the down-regulated genes in PD-L1$_{CON}$ lines were mainly involved in development and cell differentiation. These gene sets were also enriched for the melanin biosynthesis pathway (Figures 3C and S10). In contrast, the up-regulated genes were significantly implicated in several cancer hallmark-related activities, including epithelial-mesenchymal transition (EMT), interferon gamma response, up-regulation of the KRAS signaling pathway, hypoxia, and TNFA signaling mediated by NF-κB. In addition, these genes were highly enriched for cytokine production and signaling pathways (Figures 3D and S11). The most highly up-regulated genes (n = 58) in PD-L1$_{CON}$ cell lines were enriched for T cell differentiation (Figure S12).

Differential Methylation Affects Specific Genes; *DNMT3A* and *UHRF2* mRNA Expression Is Strongly Associated with Both Global Methylation Levels and *CD274* (PD-L1) mRNA Expression Level Changes

Next, we sought to identify specific genes that were potentially directly regulated by DNA methylation. Of the 508 DEGs, 39 genes also harbored differential methylation (Figures 4A and 4B, Table S5). The majority of these DEGs contained gene body DMFs (32 of 39), and only three genes showed differential methylation in the promoter regions (*SOX8, ESRP1*, and *CAPS*). For four genes (*DUSP1, ZNF516, PIP5KL1*, and *DMBT1*) we identified intergenic enhancer-associated DMFs, and loss of methylation in these regions accompanied the overexpression of these genes in PD-L1$_{CON}$ cells. Moreover, loss of gene body methylation in PD-L1$_{CON}$

lines was strongly positively correlated with down-regulation of gene expression and vice versa. This finding is consistent with observations that high gene body methylation is associated with high mRNA expression in the majority of genes (Aran et al., 2011; Bird, 1995; Lister et al., 2009). Several differentially expressed genes were associated with multiple DMFs, particularly in the gene body, consistent with the notion that DNA methylation was involved in regulating their mRNA expression levels in PD-L1$_{IND}$ and PD-L1$_{CON}$ cells (indicated by * in Figure 4A and Table S5).

We took advantage of the methylome and transcriptome data to more closely examine whether widespread global hypomethylation of PD-L1$_{CON}$ cell lines could be explained by the expression of methylation machinery genes (Figure 4C and additional data in Table S6). The *de novo* methylation machinery genes, *DNMT3A* and *UHRF2,* were significantly correlated with global methylome status, as well as *CD274* expression levels. The two methylation machinery genes may promote opposing effects on the RRBS methylome, as *DNMT3A* showed a positive correlation (rho = 0.62, Figure 4E), whereas *UHRF2* (an E3 ubiquitin ligase) was strongly negatively correlated (rho = −0.71, Figure 4D) with global methylation levels. Moreover, *DNMT3A* showed significant negative correlation with *CD274* mRNA expression (rho = 0.88), whereas *UHRF2* was significantly positively correlated with *CD274* expression (rho = −0.73). In addition, these genes exhibited a significant negative correlation with each other in their mRNA profiles (rho = −0.62, p value = 0.03, Figure 4C). We then assessed protein levels using western blots and found that DNMT3A protein levels were correlated with mRNA levels across all cell lines, with a generally higher level of DNMT3A protein in the PD-L1$_{IND}$ lines compared with PD-L1$_{CON}$ lines. However, no consistent differences were observed in UHRF1 and UHRF2 protein levels between the two groups of cell lines (Figures S13 and S14). In addition, neither the methylation maintenance gene, *DNMT1*, nor genes encoding the active demethylating enzymes (*TET1, TET2* and *TET3*) or the deamination enzymes (*APOBEC3F/G*) showed any relationship with the global methylation status or PD-L1 expression (Figure S15).

PD-L1$_{CON}$ Cell Lines Exhibit Viral Mimicry and an IFN Expression Signature, Similar to that Induced by DNMT Inhibitor Drugs, Which Is a Pattern Also Observed in Melanomas in TCGA

Demethylation of the cancer genome with DNMTi drugs activates interferon/viral defense, antigen processing, presentation, and host immune genes (Chiappinelli et al., 2015; Li et al., 2014; Liu et al., 2016). In addition, de-repression of these genes is not considered a response to general cellular stress but rather is a specific response to hypomethylation events in the genome. Accordingly, the striking hypomethylation of the PD-L1$_{CON}$ cell lines prompted us to examine whether these patterns were observed in PD-L1$_{CON}$ cells. Significant up-regulation of several type I interferon-stimulated, viral mimicry genes (*IFI44, IFI27, OASL, IL29*) and genes that are upstream of the type I interferon pathway (*IFNB1* and *IRF7*) was observed in PD-L1$_{CON}$ cell lines compared with the PD-L1$_{IND}$ lines (Figure 5A). High innate expression of several genes in PD-L1$_{CON}$ cell lines has been reported to be responsive to DNA-demethylating drugs in other studies (indicated in the box in Figure 5A) (Chiappinelli et al., 2015; Liu et al., 2016). Furthermore, DNMTi treatment has been reported to trigger cytosolic sensing of double-stranded RNA (dsRNA), causing a type I interferon response and apoptosis (Chiappinelli et al., 2015). Consistent with these findings, we observed relatively high mRNA expression of the dsRNA sensor RIG-I (*DDX58*) (the mean $\log_2$ fold increase in expression of *DDX58* was 4.96 between PD-L1$_{CON}$ and PD-L1$_{IND}$ cell lines compared with the mean $\log_2$ fold increase in expression of *CD274*, which was 6.11), as well as upstream transcriptional activators, including *IRF1*, in PD-L1$_{CON}$ cell lines. DDX58 induces IFNB1 by signaling through mitochondrial proteins. However, we did not observe a difference in the expression of *TLR3* (another dsRNA sensor). These findings may be related to the innate hypomethylation phenotype in PD-L1$_{CON}$ cells.

To examine if the gene expression patterns we observed in PD-L1$_{CON}$ cell lines were also observed in melanoma tumors, we analyzed RNA-seq data from TCGA-SKCM patients. We used the same group 1 (representative of inducible) and group 2 (representative of constitutive) melanoma cohorts as described in the previous section. Similar to our findings in PD-L1$_{IND}$ and PD-L1$_{CON}$ cell lines, we identified the trend of significant up-regulation of viral mimicry and immune response genes in group 2 patients compared with group 1 patients with melanoma, including 11 viral mimicry genes that were significantly up-regulated in group 2 patients compared with group 1 (after FDR adjustment at 5% and $\log_2$ fold change of 0.5, indicated as * in Figure 5B).

As these data suggest that global hypomethylation in PD-L1$_{CON}$ melanoma cells induces the viral mimicry pathway, including activation of human endogenous retrovirus (HERV) genes, to explore this further we

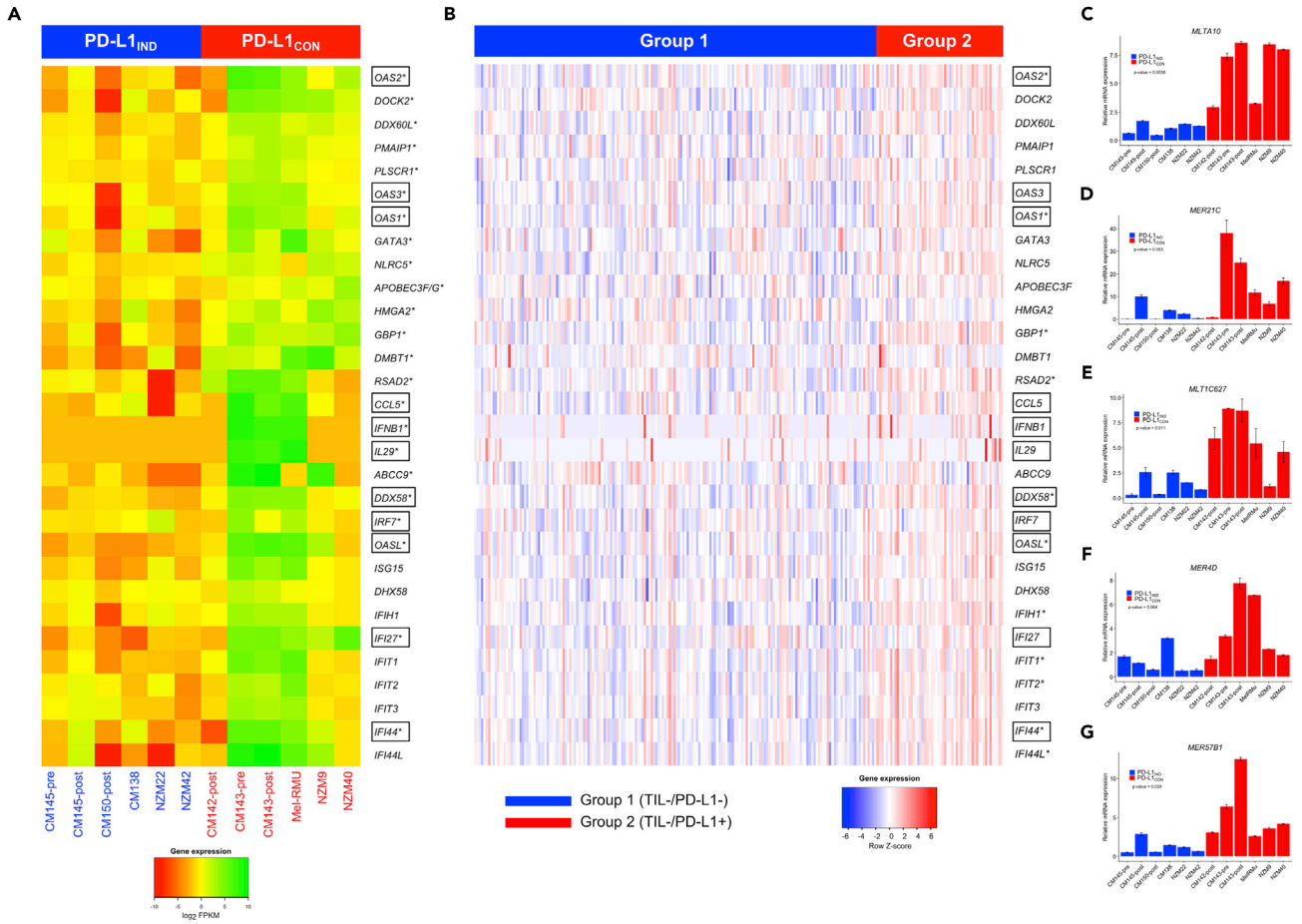

Figure 5. Expression Pattern of Viral Mimicry Genes in PD-L1$_{IND}$ and PD-L1$_{CON}$ Cell Lines and Patients with Melanoma

(A) Mean-centered heatmap of the expression level (log_2 FPKMs) of 30 viral mimicry and immune-system-related genes in PD-L1$_{IND}$ and PD-L1$_{CON}$ cell lines.

(B) Heatmap of the expression level (scaled *Z* score) of the same set of 30 genes in TCGA skin cutaneous melanoma data stratified by TIL−/PD-L1− (group 1, representative of inducible in patient group) or TIL−/PD-L1+ (group 2, representative of constitutive in patient group). In both (A) and (B), significantly differentially expressed genes are indicated with an asterisk (*) and the gene names in a box are DNMTi-responsive genes (i.e., previously shown to be silenced and re-expressed upon DNMTi treatment in cancer).

(C–G) Gene expression of five of the nine selected ERV genes as measured by RT-qPCR. There is a higher expression of five ERV genes (MLTA10, MER21C, MLT1C627, MER4D, MER57B1) in the PD-L1$_{CON}$ cell lines compared with the PD-L1$_{IND}$ group. Error bars represent SE of two technical replicates.

See also Tables S6 and S7.

used RT-qPCR to measure the expression of nine HERV genes that were previously identified to be up-regulated in a colorectal cancer cell line upon DNMTi treatment (Roulois et al., 2015). Indeed, the expression of five of these nine HERV genes was higher in the PD-L1$_{CON}$ cell lines compared with the PD-L1$_{IND}$ cell lines (Figures 5C–5G). This included *MLTA10* (mean-fold increase = 5.8, p value = 0.0038), *MER21C* (mean fold increase = 5.8, p value = 0.053), *MLT1C627* (mean-fold increase = 4.2, p value = 0.011), *MER4D* (mean-fold increase = 3.1, p value = 0.064), and *MTL2B4* (mean-fold increase = 4.4, p value = 0.039). Therefore, these data are consistent with the notion that an innate hypomethylated state is associated with the up-regulation of HERV genes together with the activation of a viral mimicry response and increased PD-L1 levels.

Global Demethylation with DNMTi Treatment Induces PD-L1 Expression, an Effect that Is Particularly Pronounced in Inducible Melanoma Cell Lines

Finally, we hypothesized that, if global hypomethylation regulates PD-L1 expression, then reducing genomic methylation levels will lead to enhanced PD-L1 expression, particularly in the inducible lines (PD-L1$_{IND}$), as they exhibited higher genomic methylation levels. We treated 12 melanoma cell lines with

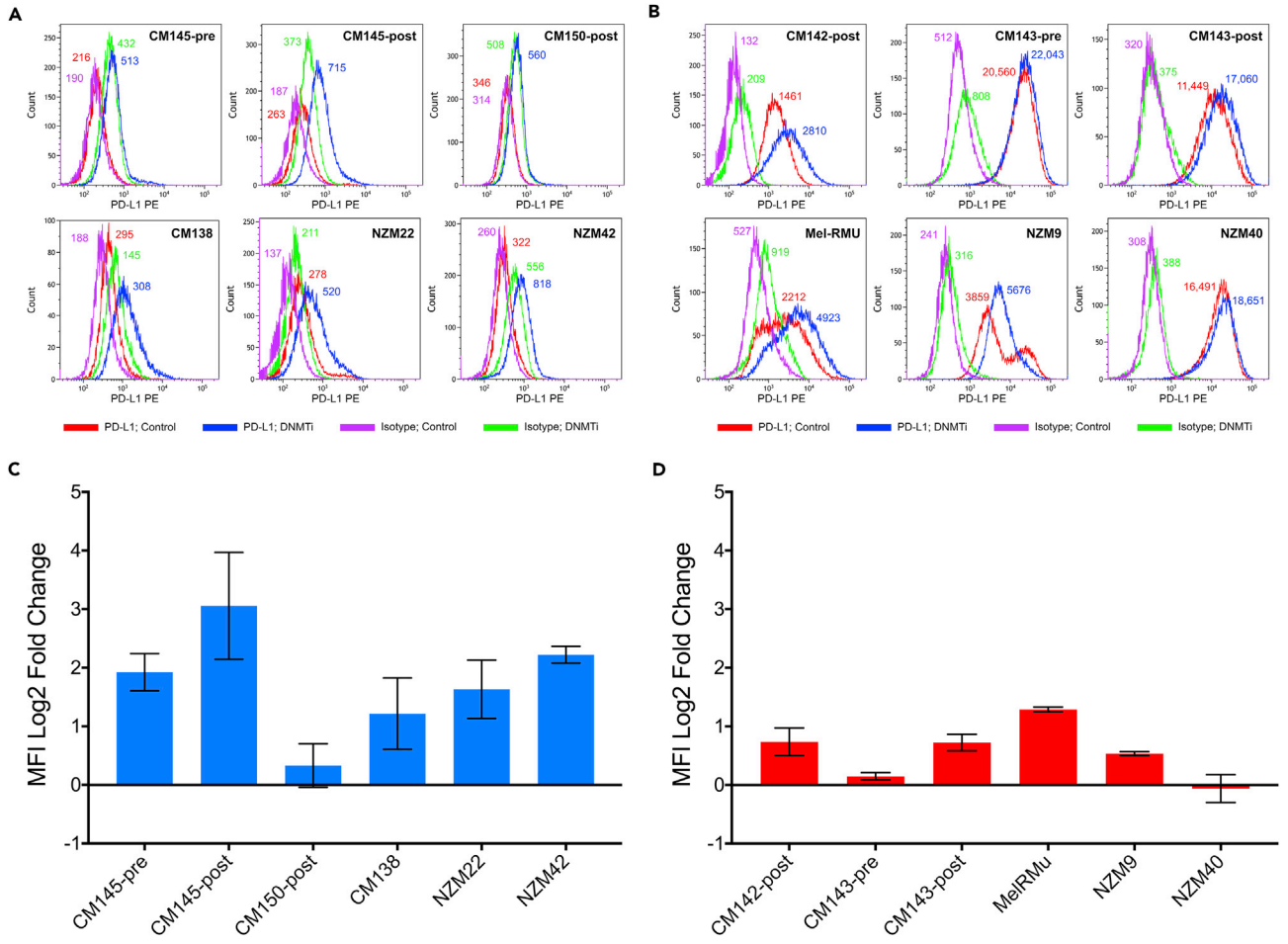

Figure 6. Up-regulation of PD-L1 Cell Surface Expression Upon DNMTi (Demethylation) Treatment in PD-L1$_{IND}$ and PD-L1$_{CON}$ Cell Lines

Flow cytometry analysis for PD-L1$_{IND}$ (A) and PD-L1$_{CON}$ (B) cell lines was performed at day 6 following 3 days treatment with decitabine (DNMTi; 0.5μM) or mock treatment (DMSO). Changes of PD-L1 expression between DNMTi treated and the control for PD-L1$_{IND}$ (C) and PD-L1$_{CON}$ (D) cell lines were calculated using medium fluorescence intensities (MFI) and the formula $\log_2$ ([(MFI$_{antibody,\ treated}$)−(MFI$_{isotype,\ treated}$)]/[(MFI$_{antibody,\ mock}$)−(MFI$_{isotype,\ mock}$)]) (Wrangle et al., 2013). Error bars represent SE of two technical replicates. See also Figures S16 and S17.

decitabine (DNMTi treatment causing global demethylation) and observed up-regulation of cell surface PD-L1 expression upon DNMTi treatment in all 12 cell lines, although the degree of up-regulation varied. Inducible lines showed stronger induction and higher up-regulation of PD-L1 expression upon demethylation compared with constitutive lines (Figures 6A–6D). In five of the six inducible cell lines, cell surface PD-L1 levels were up-regulated >2 fold and particularly in CM145-pre, CM145-post, and NZM42, which showed an average fold increase of 3.9, 10.0, and 4.7, respectively (Figure 6C). The PD-L1$_{CON}$ lines also generally showed PD-L1 up-regulation. However, as they were already expressing high levels of PD-L1, the degree of change was relatively small compared with that of the inducible lines (Figures 6C and 6D). Among the PD-L1$_{CON}$ lines, only Mel-RMU showed >2-fold (2.44) up-regulation of PD-L1 upon demethylation (Figure 6D). These patterns were true for low (100 nM) and moderate (500 nM) doses of decitabine. By western blot, total PD-L1 protein levels were up-regulated by decitabine treatment in two PD-L1$_{CON}$ lines, although in PD-L1$_{IND}$ lines, despite observing an increase in *CD274* mRNA levels after decitabine treatment (data not shown) and an increase in cell surface PD-L1 levels (see Figure 1), total PD-L1 protein levels were not generally increased upon decitabine treatment, which may be due to the relatively high levels of decitabine-induced cell death in these cells (Figure S16). In addition, we treated these cell lines with vitamin C, which promotes viral mimicry (Liu et al., 2016) and induces active demethylation by enhancing TET enzyme activity; however, this treatment did not result in any significant further increase of cell surface PD-L1 expression in either the inducible or constitutive lines, except in the inducible cell line CM145-post, which showed a 2.06 average fold increase in PD-L1 upon vitamin C treatment (Figure S17).

DISCUSSION

The success of immunotherapy, based on the inhibition of the PD1 checkpoint in lymphocytes with mAbs against PD1 or PD-L1, has focused attention on the regulation of PD-L1 expression on cancer cells. In previous investigations, we and others have defined many of the mechanisms involved in inducible PD-L1 expression on melanoma but we have not previously defined the basis for constitutive forms of PD-L1 expression (Gowrishankar et al., 2015; Madore et al., 2016). In the present study, we have examined whether DNA methylation plays a functional role in the regulation of constitutive PD-L1 expression by using sequencing-based genome-wide DNA methylation profiling combined with whole transcriptome profiling.

Constitutive PD-L1 Expression in Melanoma Is Associated with Global Hypomethylation and Transcriptomic Up-Regulation

Using RRBS genome-wide methylation profiling we identified a striking global loss of methylation between cell lines with constitutive PD-L1 expression, compared to inducible PD-L1 lines. The large methylation differences, which were distinctly identified by RRBS analysis, were confined mainly to intergenic and intronic regions, rather than promoter regions. In contrast, the same pattern of methylation differences could not be detected in the TCGA 450K melanoma methylation data, which we argue is because probes in the 450K platform were mainly located in gene promoters, whereas relatively few 450K probes were located in the gene body or intergenic regions. By RRBS analysis many genomic regions exhibiting strongly divergent methylation patterns were identified between the inducible and constitutive cell lines. These RRBS methylation patterns were remarkably similar within a group (inducible or constitutive), which we hypothesize is the result of a unified mechanism leading to hypomethylation of particular genomic regions across all the PD-L1 constitutively expressing cell lines. Consistent with previously reported data, we found the *CD274* promoter was unmethylated (Chatterjee et al., 2016), with no evidence of differential methylation occurring in the core promoter itself, which argues against methylation of the *CD274* promoter being involved in constitutive PD-L1 expression. In addition, blocking IFN-γ or interferon type I or type II with antibodies did not inhibit constitutive PD-L1 expression but (surprisingly) consistently enhanced constitutive PD-L1 expression. As expected, the same treatment with IFN-γ-blocking antibodies was able to strongly suppress interferon-driven PD-L1 induction in PD-L1$_{IND}$ cell lines. These results argue against the notion of autocrine interferon-dependent regulation of PD-L1 expression in PD-L1$_{CON}$ cells.

Transcriptome profiles in these cell lines correlated with global methylome status, and DEGs were highly up-regulated in the constitutive lines, consistent with their genomic hypomethylated state. Up-regulated genes in the PD-L1$_{CON}$ lines were associated with EMT, KRAS signaling, hypoxia, and NF-κB signaling, consistent with the known key pathways that regulate PD-L1 transcription (Chen et al., 2016). The constitutive up-regulation of these pathways as a result of global hypomethylation could be a causative factor associated with constitutive PD-L1 expression.

Of 557 differentially expressed genes, only 39 showed significant changes in methylation, with methylation differences mainly occurring in the gene body or enhancer regions associated with these genes. This suggests that, rather than promoter methylation differences, large genomic methylation differences outside the promoter regions could play a regulatory role in promoting the constitutive versus inducible PD-L1 expression. Interestingly, although global hypomethylation was correlated with mRNA up-regulation in PD-L1$_{CON}$ lines, for the majority of candidate genes, loss of gene body methylation was linked with their down-regulation in the PD-L1$_{CON}$ cell lines. This analysis identified methylation in several candidates that have the potential to regulate PD-L1 and therefore potentially could play a role in melanoma biology. For example, *IRF4, ESPR1*, and *DAPK1* showed notable down-regulation of expression and loss of gene body methylation in PD-L1$_{CON}$ cell lines. *IRF4* is upstream of the PD-L1 signaling pathway, and reduced levels of the IRF4 transcription factor lead to up-regulation of PD-L1 expression and promote T cell dysfunction (Wu et al., 2017). In addition, in TCGA patients with melanoma, reduced levels of *ESRP1* (which encodes a master splicing regulator involved in EMT) were correlated with increased immune checkpoint expression (PD-L1 and CTLA4) and elevated tumor-associated immune cytolytic activity (Yao et al., 2016). In addition, reduced levels of *DAPK1* were shown to be associated with reduced sensitivity to BRAF inhibitor therapy, suggesting its possible role in targeted melanoma therapy (Xie et al., 2017). These candidates and other genes containing multiple DMFs and deregulated gene expression warrant future investigation in the context of PD-L1 to elucidate their mechanistic specific role.

Reduced Expression of DNMT3A Correlates with Global Hypomethylation in PD-L1 Constitutive Melanomas

Global hypomethylation is perhaps the most accepted epigenetic paradigm in cancer (Baylin and Jones, 2011), yet the mechanisms involved in this are not completely clear. Our study offers fresh insights into the possible mechanisms for global hypomethylation in melanoma cell lines. The *de novo* methylating enzyme DNMT3A was strongly negatively correlated at mRNA and protein levels with PD-L1 expression and was positively associated with globally elevated methylation levels, which is consistent with the notion that hypomethylation in PD-L1$_{CON}$ cell lines may be the result of reduced levels of DNMT3A. Additional investigations are required to determine whether DNMT3A indeed plays a central role in the global hypomethylation and levels of PD-L1 expression in PD-L1$_{CON}$ cells.

We additionally observed that mRNA expression of *UHRF2*, an E3 ligase that degrades DNMT3A, was positively correlated with *CD274* levels and negatively correlated with *DNMT3A* expression and global methylation. UHRF2 has been previously reported to be a potential mediator of global hypomethylation (Jia et al., 2016), and a recent study indicated that UHRF1 and UHRF2 negatively regulate *de novo* DNA methylation by promoting DNMT3A degradation (Jia et al., 2016). UHRF2 protein expression levels in our western blots were not correlated with changes in global methylation or PD-L1 expression, although additional investigations of the relationship between UHRF2, DNMT3A, PD-L1, and global hypomethylation in melanoma may still be warranted.

Two other mechanisms that could potentially drive global hypomethylation in melanoma are direct methylation deamination (by the deaminase family gene *APOBEC* [Cortellino et al., 2011; Kumar et al., 2014]) and active removal of methylation via TET enzymes (Guo et al., 2011; Ito et al., 2011). Expression of the *APOBEC3F/G* gene was positively correlated with *CD274* expression; however, it was not strongly related with global methylation levels. Furthermore, active demethylation by TET enzymes did not appear to be involved in the PD-L1$_{CON}$ DNA methylation levels, as expression patterns of the TET family genes were not correlated with global methylation levels or *CD274* expression. This is also consistent with our experimental data whereby treatment with vitamin C failed to induce significant up-regulation of cell surface PD-L1 expression, whereas DNMTi treatment significantly increased cell surface PD-L1 levels. Taken together, our data provide evidence that *de novo* regulation of global methylation levels in melanoma is potentially part of the mechanisms regulating PD-L1 expression.

We identified, in addition to methylation of regulatory genes, several chromatin-modifying factors (e.g., *KDM4C* and *PRDM* family genes), histone-modifying genes (e.g., *CDK9, HMG20B*), and chromatin-remodeling genes (*INO80*) that were associated with PD-L1 expression and global methylome status. A recent study demonstrated transcriptional rewiring resulting from chromatin remodeling in exhausted T cells following PD-L1 blockade (Pauken et al., 2016). This epigenetic rewiring resulted in their failure to become memory T cells in the presence of high antigen levels. Moreover, evidence for global chromatin remodeling during melanoma progression is emerging (Fiziev et al., 2017). For example, *INO80* was recently shown to reduce nucleosome occupancy and promote oncogenic transcription in melanoma (Zhou et al., 2016). It is plausible that these genes contribute to differential chromatin remodeling and lead to alterations in the epigenetic landscape in PD-L1$_{IND}$ and PD-L1$_{CON}$ cell lines, and our data provide a basis for exploring the role of chromatin and histone changes in determining PD-L1 expression in tumors.

We reasoned that one possible explanation for the association between the global hypomethylation and constitutive PD-L1 expression is that global hypomethylation results in changes in the signaling pathways involved in immune response and generation of a constant "on" signal. For example, this could include the hypomethylation and activation of stimulator of IFN genes (STING), an adaptor protein associated with the ER (Corrales et al., 2016, 2017). STING was reported to be defective in many types of cancer. In colon cancer, for example, this results from methylation of genes encoding STING or other proteins in the pathway (Xia et al., 2016a). Similar studies in melanoma cell lines have shown loss of STING in 3/11 lines and of cGAS (the synthase generating cyclic dinucleotides) in 4/11 lines. Immunohistochemical (IHC) studies showed that over 40% of metastases lacked STING or cGAS expression (Xia et al., 2016b). Proteins downstream of STING, such as IRF3 and NF-κB, were also lost in some cell lines. STING is not involved in the response to dsRNA. Nevertheless, cGAS has been reported to be essential for the response to immune checkpoint blockade in B16 mouse melanoma studies (Wang et al., 2017).

DNMTi Treatment Increases PD-L1 Expression, Which like Constitutive PD-L1 Expression in Melanoma, Is Associated with a Viral Mimicry Phenotype

Studies in epithelial cancers have shown that treatment with DNMTi can induce an IFN gene signature response in the cells, including PD-L1 (Li et al., 2014). The latter was suggested to be due to viral mimicry (Roulois et al., 2015) resulting from demethylation of human endogenous retroviral sequences (HERVs), which were then recognized by dsRNA sensors *TLR3*, *MGA5*, and *RIGI* in the cells (Chiappinelli et al., 2015, 2016). This is consistent with our findings that repeat elements, particularly the HERVs, were strongly hypomethylated in the PD-L1$_{CON}$ cells and that their mRNA expression levels were increased, higher in PD-L1$_{CON}$ than in PD-L1$_{IND}$ cells. Moreover, the hypomethylation phenotype was associated with the up-regulation of genes responsible for generating endogenous immune responses in cancer cells treated with DNMTi, such as several type I interferon-stimulated, viral mimicry-related genes (*IFI44, IFI27, OASL, IL29*) and genes that are upstream of the type I interferon pathway (*IFNB1*, *IRF7*) in PD-L1$_{CON}$ cell lines (Chiappinelli et al., 2015; Liu et al., 2016). Analysis of TCGA melanoma patient transcriptome data revealed that these viral mimicry genes were significantly differentially expressed between constitutive (group 2) and inducible (group 1) patient groups. Taken together, these results support the notion that up-regulation of a viral mimicry phenotype is the result of global hypomethylation in PD-L1$_{CON}$ cells. Further studies are needed to confirm whether constitutive up-regulation of the type 1 IFN pathway is a result of a hypomethylation-mediated viral mimicry phenotype.

In summary, based on our results, we conclude that constitutive expression of PD-L1 is a consequence of global hypomethylation and that global DNA methylation status is an important factor in the regulation of PD-L1. The exact mechanism of how the hypomethylated state regulates pathways involved in PD-L1 expression in melanoma needs to be further investigated, but constitutive expression of PD-L1 in melanoma cells may identify melanomas that have endogenous activation of IFN signaling pathways, analogous to effects of treatment with inhibitors of DNMT enzymes. We identified that down-regulation of *DNMT3A* was associated with global hypomethylation and PD-L1 expression. Further studies are needed to examine whether this subset of melanomas have similar responses to PD1 checkpoint inhibitor treatments or if they require combination therapies that target other consequences of hypomethylation, such as activation of epithelial mesenchymal transition, NF-κB, or hypoxia pathways.

METHODS

All methods can be found in the accompanying Transparent Methods supplemental file

DATA AND SOFTWARE AVAILABILITY

DNA methylation and transcriptomic data for PD-L1$_{CON}$ and PDL1$_{IND}$ cell lines are available at Database: NCBI GEO, accession number GSE107622.

SUPPLEMENTAL INFORMATION

Supplemental Information includes Transparent Methods, 17 figures, and 7 tables and can be found with this article online at https://doi.org/10.1016/j.isci.2018.05.021.

ACKNOWLEDGMENTS

The authors thank Anna Leichter for technical assistance with cell culture. This work was supported by the New Zealand Institute for Cancer Research Trust, the Maurice Wilkins Center for Molecular Biodiscovery, the Marsden Fund, Healthcare Otago Charitable Trust, Genesis Oncology Trust, Maurice and Phyllis Paykel Trust, Dunedin School of Medicine Bequest, and a University of Otago Research Grant, as well as the Melanoma Institute of Australia, and an Australian National Health and Medical Research Council (NHMRC) program grant 633004.

AUTHOR CONTRIBUTIONS

Conceptualization, A.C., E.J.R., J.M., S.J.G., J.T., M.R.E., and P.H.; Methodology, A.C., S.J.G., E.S., J.T., E.J.R., A.A., and J.M.; Investigation, A.C., E.J.R., A.A., J.M., S.J.G., E.S., and J.T.; Formal analysis, A.C., E.J.R., A.A., P.A.S., M.P., J.M., S.J.G., E.S., and J.T.; Writing – Original Draft, A.C. and M.R.E.; Writing – Review and Editing, A.C., E.J.R., P.S., S.J.G., J.T., M.R.E., and P.H.; Visualization, A.C., E.J.R., A.A., S.J.G., and

J.T.; Funding Acquisition, M.R.E., P.H., S.J.G., A.C., and E.J.R.; Resources, P.H., A.C., and M.R.E.; Supervision, M.R.E., P.H., and A.C.

DECLARATION OF INTERESTS

The authors declare no competing interests.

Received: December 22, 2017
Revised: May 8, 2018
Accepted: May 29, 2018
Published: June 28, 2018

REFERENCES

Ansell, S.M., Lesokhin, A.M., Borrello, I., Halwani, A., Scott, E.C., Gutierrez, M., Schuster, S.J., Millenson, M.M., Cattry, D., Freeman, G.J., et al. (2015). PD-1 blockade with nivolumab in relapsed or refractory Hodgkin's lymphoma. N. Engl. J. Med. *372*, 311–319.

Aran, D., Toperoff, G., Rosenberg, M., and Hellman, A. (2011). Replication timing-related and gene body-specific methylation of active human genes. Hum. Mol. Genet. *20*, 670–680.

Baylin, S.B., and Jones, P.A. (2011). A decade of exploring the cancer epigenome - biological and translational implications. Nat. Rev. Cancer *11*, 726–734.

Bird, A.P. (1995). Gene number, noise reduction and biological complexity. Trends Genet. *11*, 94–100.

Chatterjee, A., Macaulay, E.C., Ahn, A., Ludgate, J.L., Stockwell, P.A., Weeks, R.J., Parry, M.F., Foster, T.J., Knarston, I.M., Eccles, M.R., et al. (2017a). Comparative assessment of DNA methylation patterns between reduced representation bisulfite sequencing and sequenom EpiTyper methylation analysis. Epigenomics *9*, 823–832.

Chatterjee, A., Rodger, E.J., Stockwell, P.A., Le Mee, G., and Morison, I.M. (2017b). Generating multiple base-resolution DNA methylomes using reduced representation bisulfite sequencing. Methods Mol. Biol. *1537*, 279–298.

Chatterjee, A., Stockwell, P.A., Rodger, E.J., Parry, M.F., and Eccles, M.R. (2016). scan_tcga tools for integrated epigenomic and transcriptomic analysis of tumor subgroups. Epigenomics *8*, 1315–1330.

Chen, J., Jiang, C.C., Jin, L., and Zhang, X.D. (2016). Regulation of PD-L1: a novel role of pro-survival signalling in cancer. Ann. Oncol. *27*, 409–416.

Chiappinelli, K.B., Strissel, P.L., Desrichard, A., Li, H., Henke, C., Akman, B., Hein, A., Rote, N.S., Cope, L.M., Snyder, A., et al. (2015). Inhibiting DNA methylation causes an interferon response in cancer via dsRNA including endogenous retroviruses. Cell *162*, 974–986.

Chiappinelli, K.B., Zahnow, C.A., Ahuja, N., and Baylin, S.B. (2016). Combining epigenetic and immunotherapy to combat cancer. Cancer Res. *76*, 1683–1689.

Corrales, L., Matson, V., Flood, B., Spranger, S., and Gajewski, T.F. (2017). Innate immune signaling and regulation in cancer immunotherapy. Cell Res. *27*, 96–108.

Corrales, L., McWhirter, S.M., Dubensky, T.W., Jr., and Gajewski, T.F. (2016). The host STING pathway at the interface of cancer and immunity. J. Clin. Invest. *126*, 2404–2411.

Cortellino, S., Xu, J., Sannai, M., Moore, R., Caretti, E., Cigliano, A., Le Coz, M., Devarajan, K., Wessels, A., Soprano, D., et al. (2011). Thymine DNA glycosylase is essential for active DNA demethylation by linked deamination-base excision repair. Cell *146*, 67–79.

Daud, A.I., Wolchok, J.D., Robert, C., Hwu, W.J., Weber, J.S., Ribas, A., Hodi, F.S., Joshua, A.M., Kefford, R., Hersey, P., et al. (2016). Programmed death-ligand 1 expression and response to the anti-programmed death 1 antibody pembrolizumab in melanoma. J. Clin. Oncol. *34*, 4102–4109.

Dong, H., Zhu, G., Tamada, K., Flies, D.B., van Deursen, J.M., and Chen, L. (2004). B7-H1 determines accumulation and deletion of intrahepatic CD8(+) T lymphocytes. Immunity *20*, 327–336.

Festino, L., Botti, G., Lorigan, P., Masucci, G.V., Hipp, J.D., Horak, C.E., Melero, I., and Ascierto, P.A. (2016). Cancer treatment with anti-PD-1/PD-L1 agents: is PD-L1 expression a biomarker for patient selection? Drugs *76*, 925–945.

Fiziev, P., Akdemir, K.C., Miller, J.P., Keung, E.Z., Samant, N.S., Sharma, S., Natale, C.A., Terranova, C.J., Maitituoheti, M., Amin, S.B., et al. (2017). Systematic epigenomic analysis reveals chromatin states associated with melanoma progression. Cell Rep. *19*, 875–889.

Gallagher, S.J., Mijatov, B., Gunatilake, D., Gowrishankar, K., Tiffen, J., James, W., Jin, L., Pupo, G., Cullinane, C., McArthur, G.A., et al. (2014). Control of NF-kB activity in human melanoma by bromodomain and extra-terminal protein inhibitor I-BET151. Pigment Cell Melanoma Res. *27*, 1126–561137.

Gandini, S., Massi, D., and Mandala, M. (2016). PD-L1 expression in cancer patients receiving anti PD-1/PD-L1 antibodies: a systematic review and meta-analysis. Crit. Rev. Oncol. Hematol. *100*, 88–98.

Gowrishankar, K., Gunatilake, D., Gallagher, S.J., Tiffen, J., Rizos, H., and Hersey, P. (2015). Inducible but not constitutive expression of PD-L1 in human melanoma cells is dependent on activation of NF-kappaB. PLoS One *10*, e0123410.

Greenwald, R.J., Freeman, G.J., and Sharpe, A.H. (2005). The B7 family revisited. Annu. Rev. Immunol. *23*, 515–548.

Guo, J.U., Su, Y., Zhong, C., Ming, G.L., and Song, H. (2011). Hydroxylation of 5-methylcytosine by TET1 promotes active DNA demethylation in the adult brain. Cell *145*, 423–434.

Hersey, P., and Gowrishankar, K. (2015). Pembrolizumab joins the anti-PD-1 armamentarium in the treatment of melanoma. Future Oncol. *11*, 133–140.

Hodi, F.S., Chesney, J., Pavlick, A.C., Robert, C., Grossmann, K.F., McDermott, D.F., Linette, G.P., Meyer, N., Giguere, J.K., Agarwala, S.S., et al. (2016). Combined nivolumab and ipilimumab versus ipilimumab alone in patients with advanced melanoma: 2-year overall survival outcomes in a multicentre, randomised, controlled, phase 2 trial. Lancet Oncol. *17*, 1558–1568.

Ito, S., Shen, L., Dai, Q., Wu, S.C., Collins, L.B., Swenberg, J.A., He, C., and Zhang, Y. (2011). Tet proteins can convert 5-methylcytosine to 5-formylcytosine and 5-carboxylcytosine. Science *333*, 1300–1303.

Jia, Y., Li, P., Fang, L., Zhu, H., Xu, L., Cheng, H., Zhang, J., Li, F., Feng, Y., Li, Y., et al. (2016). Negative regulation of DNMT3A de novo DNA methylation by frequently overexpressed UHRF family proteins as a mechanism for widespread DNA hypomethylation in cancer. Cell Discov. *2*, 16007.

Kumar, R., DiMenna, L.J., Chaudhuri, J., and Evans, T. (2014). Biological function of activation-induced cytidine deaminase (AID). Biomed. J. *37*, 269–283.

Li, H., Chiappinelli, K.B., Guzzetta, A.A., Easwaran, H., Yen, R.W., Vatapalli, R., Topper, M.J., Luo, J., Connolly, R.M., Azad, N.S., et al. (2014). Immune regulation by low doses of the DNA methyltransferase inhibitor 5-azacitidine in common human epithelial cancers. Oncotarget *5*, 587–598.

Lister, R., Pelizzola, M., Dowen, R.H., Hawkins, R.D., Hon, G., Tonti-Filippini, J., Nery, J.R., Lee, L., Ye, Z., Ngo, Q.M., et al. (2009). Human DNA methylomes at base resolution show widespread epigenomic differences. Nature *462*, 315–322.

Liu, M., Ohtani, H., Zhou, W., Orskov, A.D., Charlet, J., Zhang, Y.W., Shen, H., Baylin, S.B., Liang, G., Gronbaek, K., et al. (2016). Vitamin C increases viral mimicry induced by 5-aza-2'-deoxycytidine. Proc. Natl. Acad. Sci. USA *113*, 10238–10244.

Madore, J., Strbenac, D., Vilain, R., Menzies, A.M., Yang, J.Y., Thompson, J.F., Long, G.V., Mann, G.J., Scolyer, R.A., and Wilmott, J.S. (2016). PD-L1 negative status is associated with lower mutation burden, differential expression of immune-related genes, and worse survival in stage III melanoma. Clin. Cancer Res. *22*, 3915–3923.

Madore, J., Vilain, R.E., Menzies, A.M., Kakavand, H., Wilmott, J.S., Hyman, J., Yearley, J.H., Kefford, R.F., Thompson, J.F., Long, G.V., et al. (2014). PD-L1 expression in melanoma shows marked heterogeneity within and between patients: implications for anti-PD-1/PD-L1 clinical trials. Pigment Cell Melanoma Res. *28*, 245–253.

Meissner, A., Mikkelsen, T.S., Gu, H., Wernig, M., Hanna, J., Sivachenko, A., Zhang, X., Bernstein, B.E., Nusbaum, C., Jaffe, D.B., et al. (2008). Genome-scale DNA methylation maps of pluripotent and differentiated cells. Nature *454*, 766–770.

Pardoll, D.M. (2012). The blockade of immune checkpoints in cancer immunotherapy. Nat. Rev. Cancer *12*, 252–264.

Pauken, K.E., Sammons, M.A., Odorizzi, P.M., Manne, S., Godec, J., Khan, O., Drake, A.M., Chen, Z., Sen, D.R., Kurachi, M., et al. (2016). Epigenetic stability of exhausted T cells limits durability of reinvigoration by PD-1 blockade. Science *354*, 1160–1165.

Platanias, L.C. (2005). Mechanisms of type-I- and type-II-interferon-mediated signalling. Nat. Rev. Immunol. *5*, 375–386.

Ribas, A. (2015). Adaptive immune resistance: how cancer protects from immune attack. Cancer Discov. *5*, 915–919.

Ribas, A., Hamid, O., Daud, A., Hodi, F.S., Wolchok, J.D., Kefford, R., Joshua, A.M., Patnaik, A., Hwu, W.J., Weber, J.S., et al. (2016). Association of pembrolizumab with tumor response and survival among patients with advanced melanoma. J. Am. Med. Assoc. *315*, 1600–1609.

Roulois, D., Loo Yau, H., Singhania, R., Wang, Y., Danesh, A., Shen, S.Y., Han, H., Liang, G., Jones, P.A., Pugh, T.J., et al. (2015). DNA-demethylating agents target colorectal cancer cells by inducing viral mimicry by endogenous transcripts. Cell *162*, 961–973.

Schildberg, F.A., Klein, S.R., Freeman, G.J., and Sharpe, A.H. (2016). Coinhibitory pathways in the B7-CD28 ligand-receptor family. Immunity *44*, 955–972.

Smyth, M.J., Ngiow, S.F., Ribas, A., and Teng, M.W. (2016). Combination cancer immunotherapies tailored to the tumour microenvironment. Nat. Rev. Clin. Oncol. *13*, 143–158.

Spranger, S., and Gajewski, T.F. (2016). Tumor-intrinsic oncogene pathways mediating immune avoidance. Oncoimmunology *5*, e1086862.

Taube, J.M., Anders, R.A., Young, G.D., Xu, H., Sharma, R., McMiller, T.L., Chen, S., Klein, A.P., Pardoll, D.M., Topalian, S.L., et al. (2012). Colocalization of inflammatory response with B7-h1 expression in human melanocytic lesions supports an adaptive resistance mechanism of immune escape. Sci. Transl. Med. *4*, 127ra137.

Topalian, S.L., Taube, J.M., Anders, R.A., and Pardoll, D.M. (2016). Mechanism-driven biomarkers to guide immune checkpoint blockade in cancer therapy. Nat. Rev. Cancer *16*, 275–287.

Ugurel, S., Rohmel, J., Ascierto, P.A., Flaherty, K.T., Grob, J.J., Hauschild, A., Larkin, J., Long, G.V., Lorigan, P., McArthur, G.A., et al. (2016). Survival of patients with advanced metastatic melanoma: the impact of novel therapies. Eur. J. Cancer *53*, 125–134.

Wang, H., Hu, S., Chen, X., Shi, H., Chen, C., Sun, L., and Chen, Z.J. (2017). cGAS is essential for the antitumor effect of immune checkpoint blockade. Proc. Natl. Acad. Sci. USA *114*, 1637–1642.

Wrangle, J., Wang, W., Koch, A., Easwaran, H., Mohammad, H.P., Vendetti, F., Vancriekinge, W., Demeyer, T., Du, Z., Parsana, P., et al. (2013). Alterations of immune response of non-small cell lung cancer with azacytidine. Oncotarget *4*, 2067–2079.

Wu, J., Shi, X., Xiao, X., Minze, L., Wang, J., Ghobrial, R.M., Xia, J., Sciammas, R., Li, X.C., and Chen, W. (2017). IRF4 controls a core regulatory circuit of T cell dysfunction in transplantation. J. Immunol. *198* (1 Supplement), 124.10.

Xia, T., Konno, H., Ahn, J., and Barber, G.N. (2016a). Deregulation of STING signaling in colorectal carcinoma constrains DNA damage responses and correlates with tumorigenesis. Cell Rep. *14*, 282–297.

Xia, T., Konno, H., and Barber, G.N. (2016b). Recurrent loss of STING signaling in melanoma correlates with susceptibility to viral oncolysis. Cancer Res. *76*, 6747–6759.

Xie, J.Y., Chen, P.C., Zhang, J.L., Gao, Z.S., Neves, H., Zhang, S.D., Wen, Q., Chen, W.D., Kwok, H.F., and Lin, Y. (2017). The prognostic significance of DAPK1 in bladder cancer. PLoS One *12*, e0175290.

Yao, J., Caballero, O.L., Huang, Y., Lin, C., Rimoldi, D., Behren, A., Cebon, J.S., Hung, M.C., Weinstein, J.N., Strausberg, R.L., et al. (2016). Altered expression and splicing of ESRP1 in malignant melanoma correlates with epithelial-mesenchymal status and tumor-associated immune cytolytic activity. Cancer Immunol. Res. *4*, 552–561.

Yao, S., Zhu, Y., and Chen, L. (2013). Advances in targeting cell surface signalling molecules for immune modulation. Nat. Rev. Drug Discov. *12*, 130–146.

Zhou, B., Wang, L., Zhang, S., Bennett, B.D., He, F., Zhang, Y., Xiong, C., Han, L., Diao, L., Li, P., et al. (2016). INO80 governs superenhancer-mediated oncogenic transcription and tumor growth in melanoma. Genes Dev. *30*, 1440–1453.

ISCI, Volume *4*

Supplemental Information

Marked Global DNA Hypomethylation Is Associated with Constitutive PD-L1 Expression in Melanoma

Aniruddha Chatterjee, Euan J. Rodger, Antonio Ahn, Peter A. Stockwell, Matthew Parry, Jyoti Motwani, Stuart J. Gallagher, Elena Shklovskaya, Jessamy Tiffen, Michael R. Eccles, and Peter Hersey

Supplemental Figures:

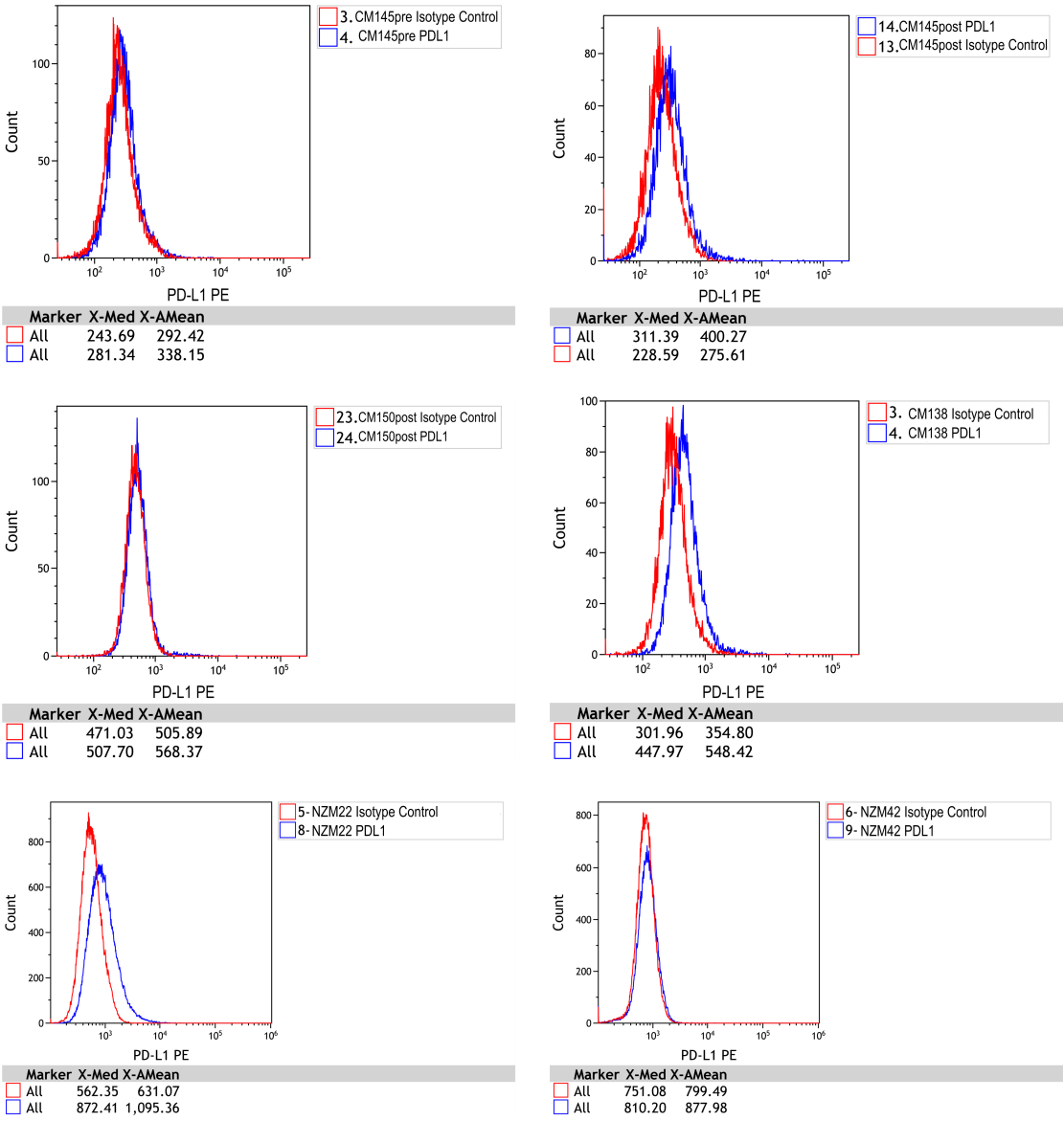

Figure S1. FACS analysis results of the PD-L1$_{IND}$ cell lines. Related to Figure 1. Flow cytometry was used to determine cell surface expression of PD-L1 in the PD-L1$_{IND}$ cell lines. The melanoma cell lines were stained with anti-PD-L1 (PE) and the isotype control antibody.

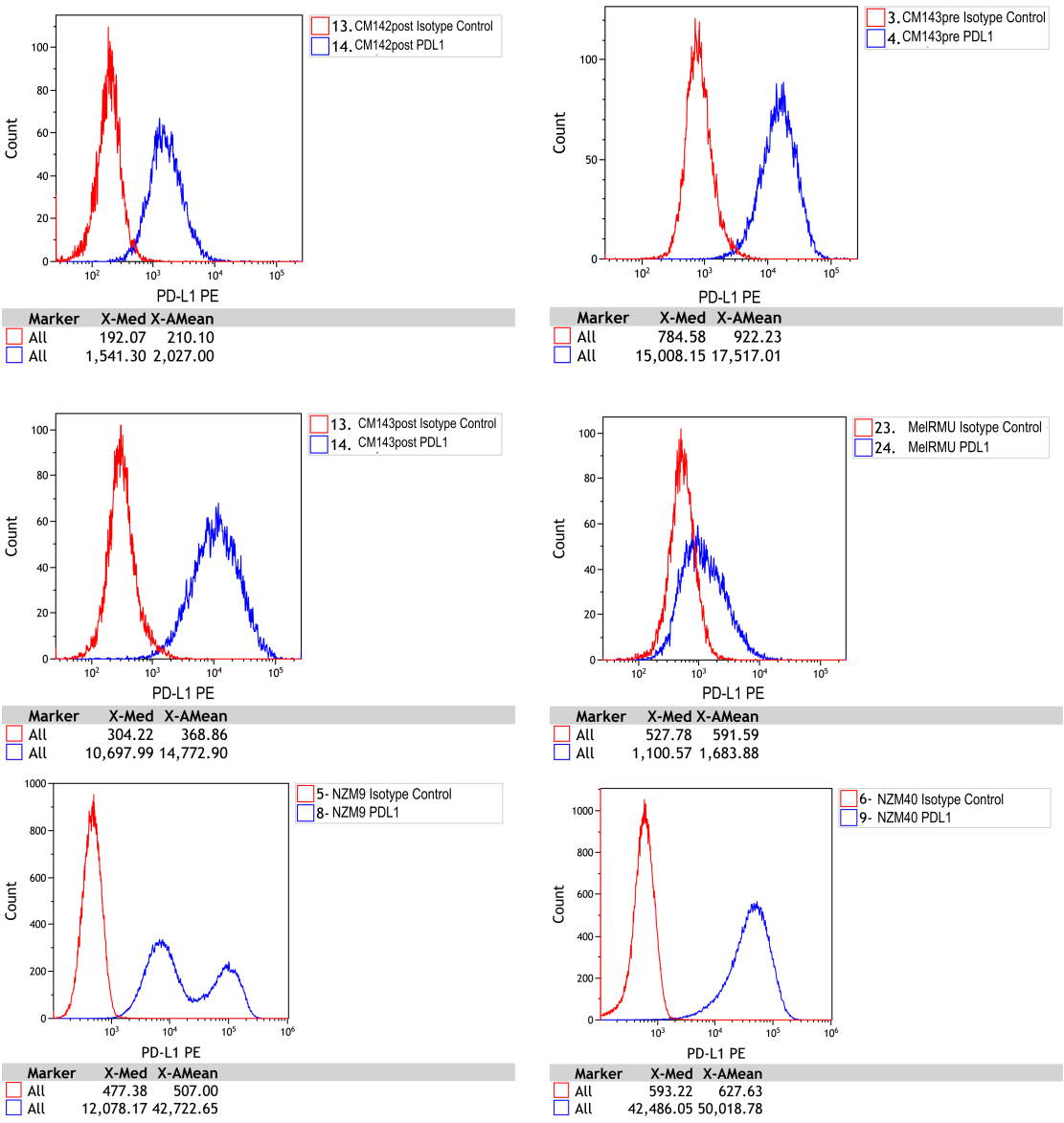

Figure S2. FACS analysis results of the PD-L1$_{CON}$ cell lines. Related to Figure 1. Flow cytometry was used to determine cell surface expression of PD-L1 in the PD-L1$_{CON}$ cell lines. The melanoma cell lines were stained with anti-PD-L1 (PE) and the isotype control antibody. An expression level of at least five-fold higher than the isotype control was considered as constitutive expression of PD-L1.

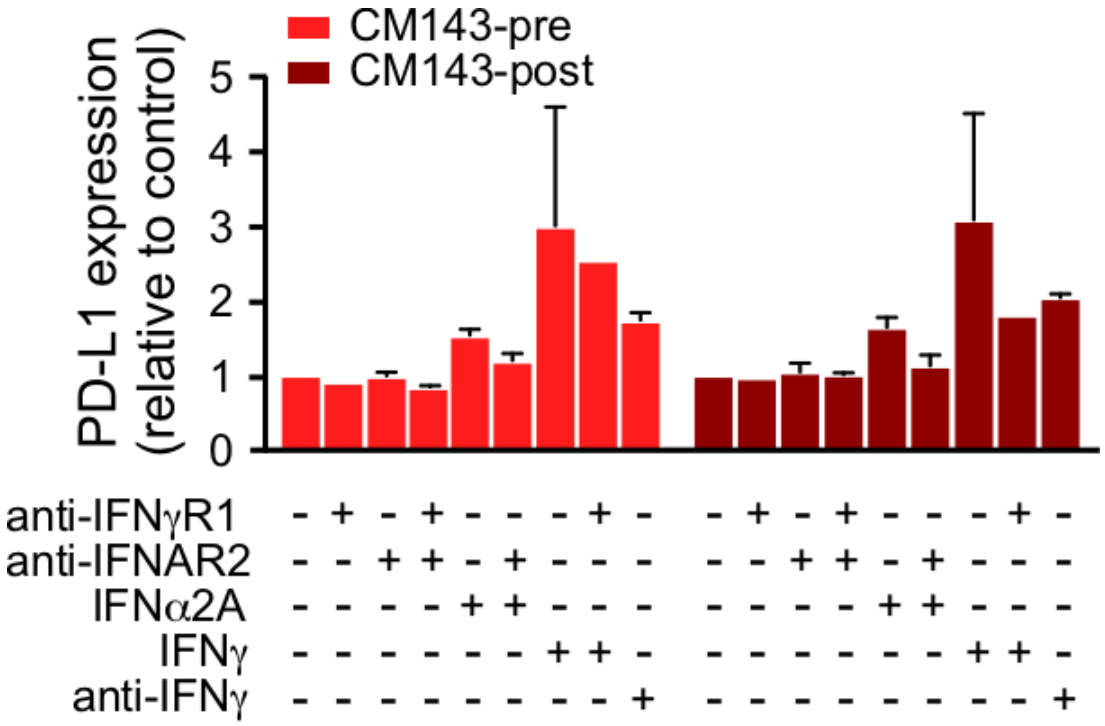

Figure S3. Blocking interferon signalling in PD-L1$_{CON}$ lines does not reduce constitutive PD-L1 expression. Related to Figure 1. Interferon-type I or -type II signaling was blocked with the indicated antibodies in the absence or presence of IFNα2A or 100ng/ml IFNγ as indicated. PD-L1 expression was measured by flow cytometry on day 3. Results are expressed relative to control (no treatment) levels. Error bars represent SE of two technical replicates.

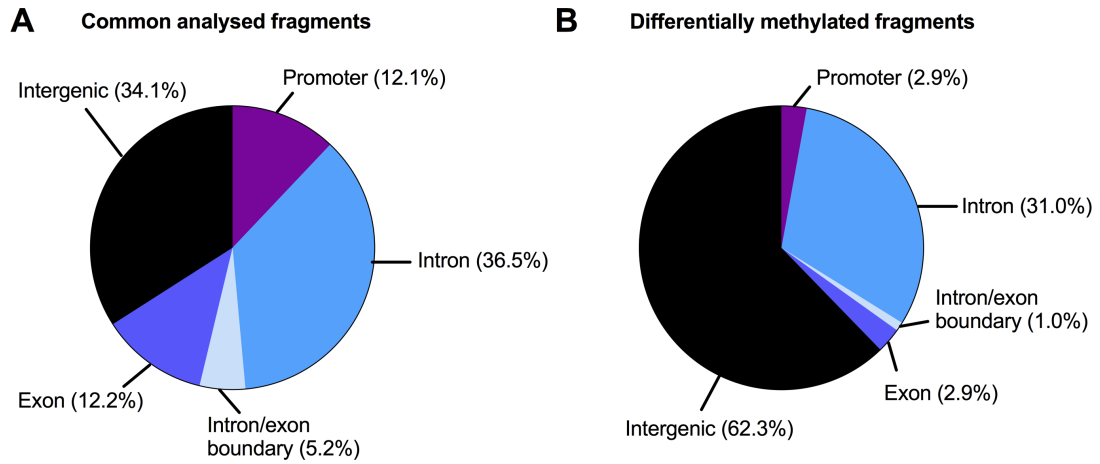

Figure S4. Genomic distribution of the analysed RRBS fragments (A) and the identified DMFs between PD-L1$_{CON}$ and PD-L1$_{IND}$ melanoma cell lines. Related to Figure 2. Gene promoters were defined as -5 to +1 kb from the TSS.

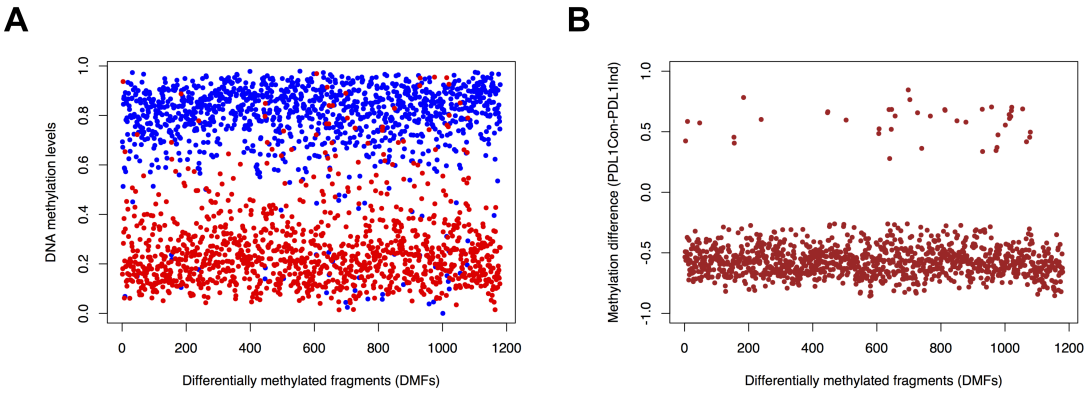

Figure S5. DNA methylation patterns (A) and mean methylation difference (B) for the identified DMFs between PD-L1$_{CON}$ and PD-L1$_{IND}$ melanoma cell lines. Related to Figure 2. All these fragments had high coverage methylation data after filtering for coverage (at least four cell lines in each group had 10 or more reads and at least 2 CpG sites in a fragment. The methylation was shown in a scale of 0 to 1.0 (i.e., 0 to 100%).

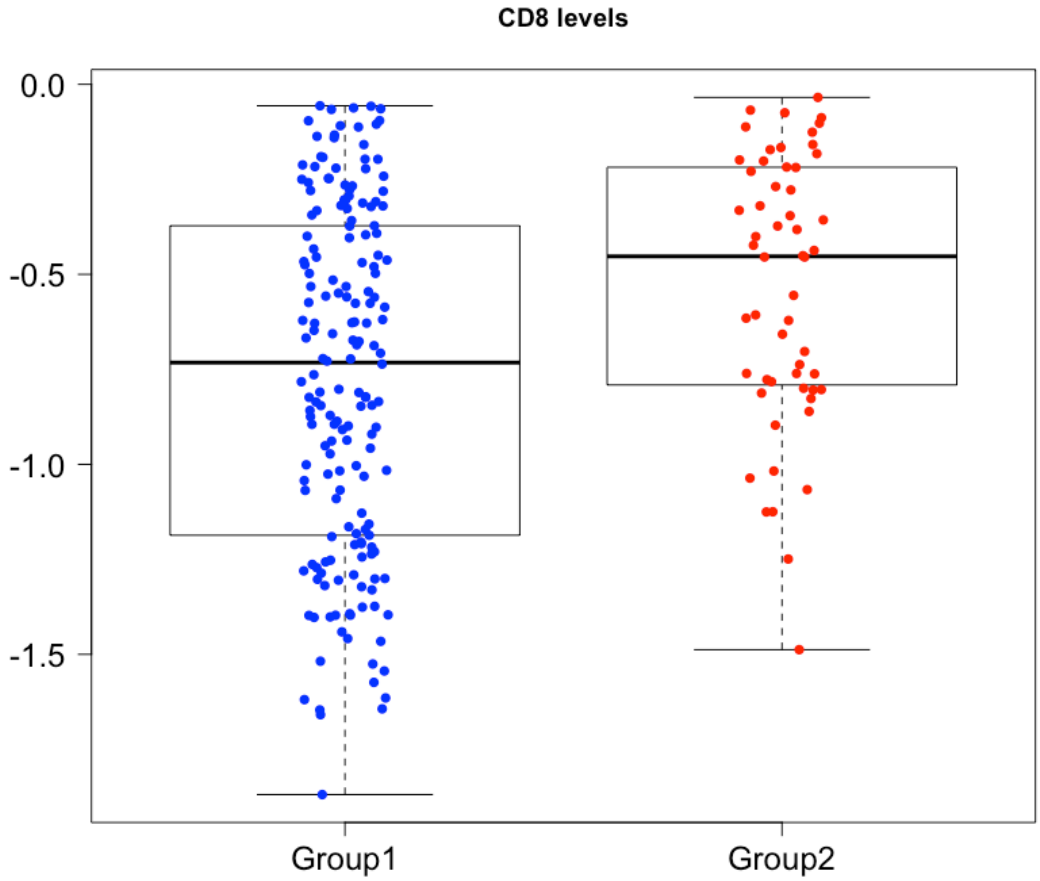

Figure S6. CD8 levels (TILs) based on immune cell deconvolution analysis on TCGA-SKCM RNA-Seq data for Group 1 and Group 2 patients (representative of PD-L1$_{IND}$ and PD-L1$_{CON}$ groups). The boxplots show the median and interquartile range. Related to Figure 2.

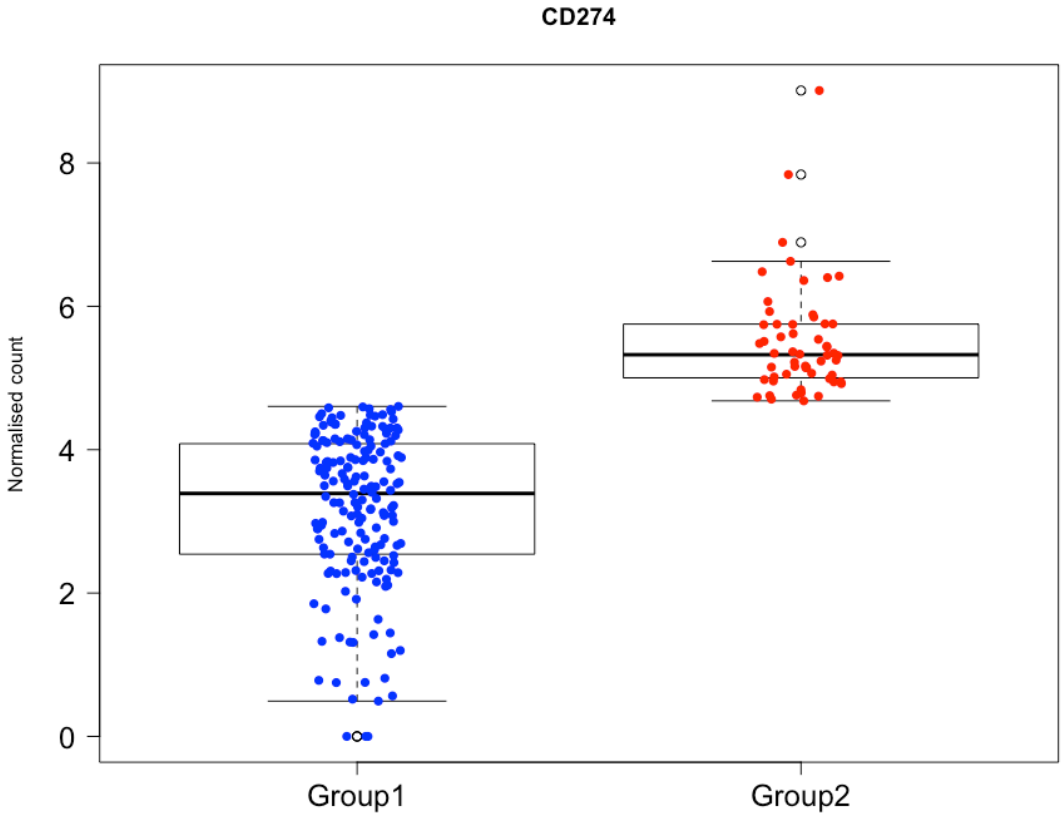

Figure S7. PD-L1 (*CD274*) mRNA levels based on TCGA-SKCM RNA-Seq data for Group 1 and Group 2 patients (representative of PD-L1$_{IND}$ and PD-L1$_{CON}$ groups). The boxplots show the median and interquartile range. Related to Figure 2.

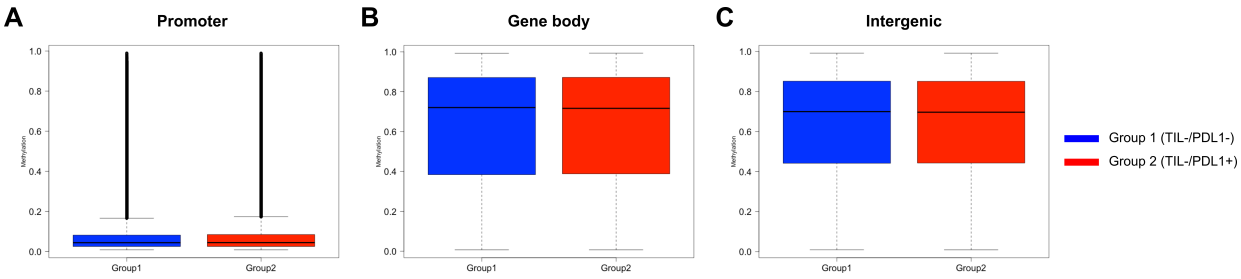

Figure S8. Methylation levels based on 450K TCGA-SKCM data for Group 1 and Group 2 patients (representative of PD-L1$_{IND}$ and PD-L1$_{CON}$ groups). Boxplots show the average beta values and interquartile range of all probes belonging to the feature. Related to Figure 2.

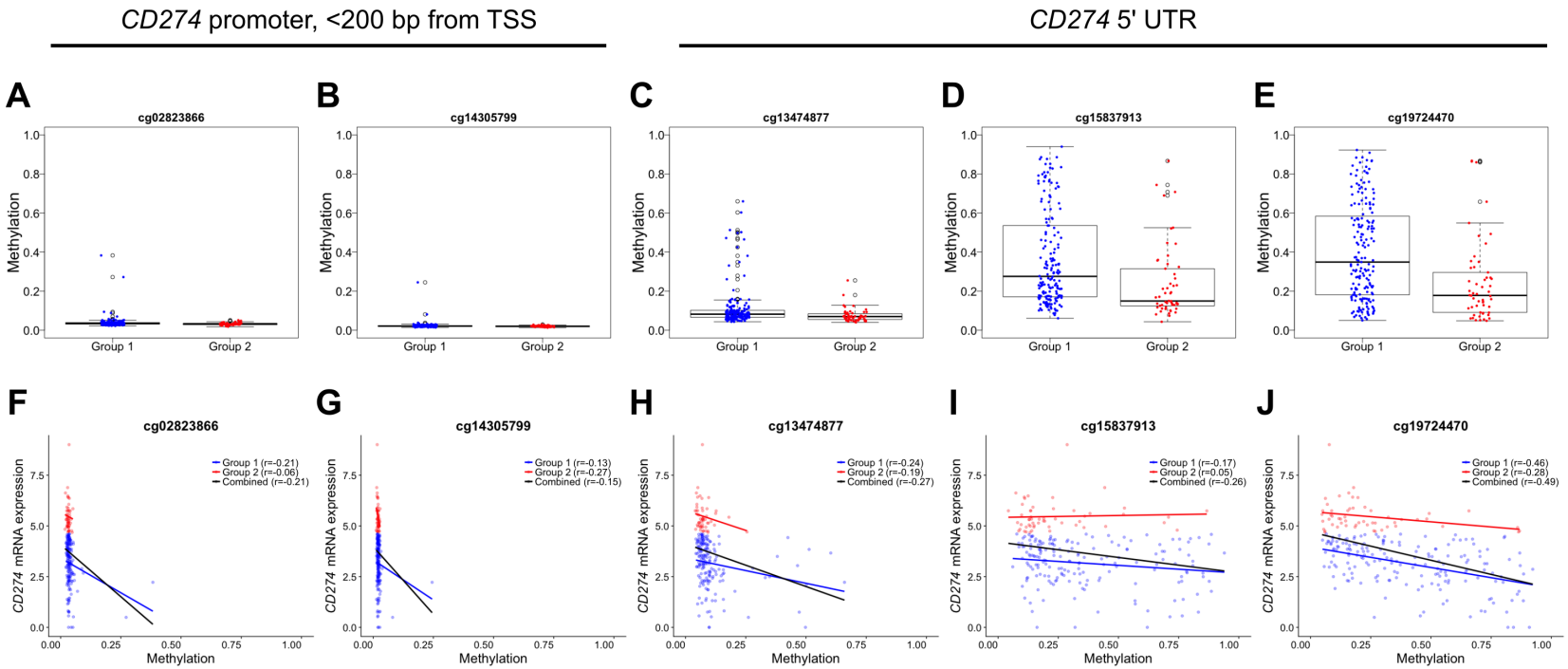

Figure S9. Methylation levels based on 450K TCGA-SKCM data for cg02823866 and cg14305799 probes for Group 1 and Group 2 patients (representative of PD-L1$_{IND}$ and PD-L1$_{CON}$ groups). Related to Figure 2. We specifically analyzed tumours that were TIL-ve to reduce the impact of immune cell signaling on tumour PD-L1 expression, and divided these tumours into Group 1 (PD-L1-ve, n= 180) and Group 2 (PD-L1+ve, n= 54). We considered these two groups (Group 1 and Group 2) as being the most representative of our analysed cell lines (PD-L1$_{IND}$ and PD-L1$_{CON}$, respectively).

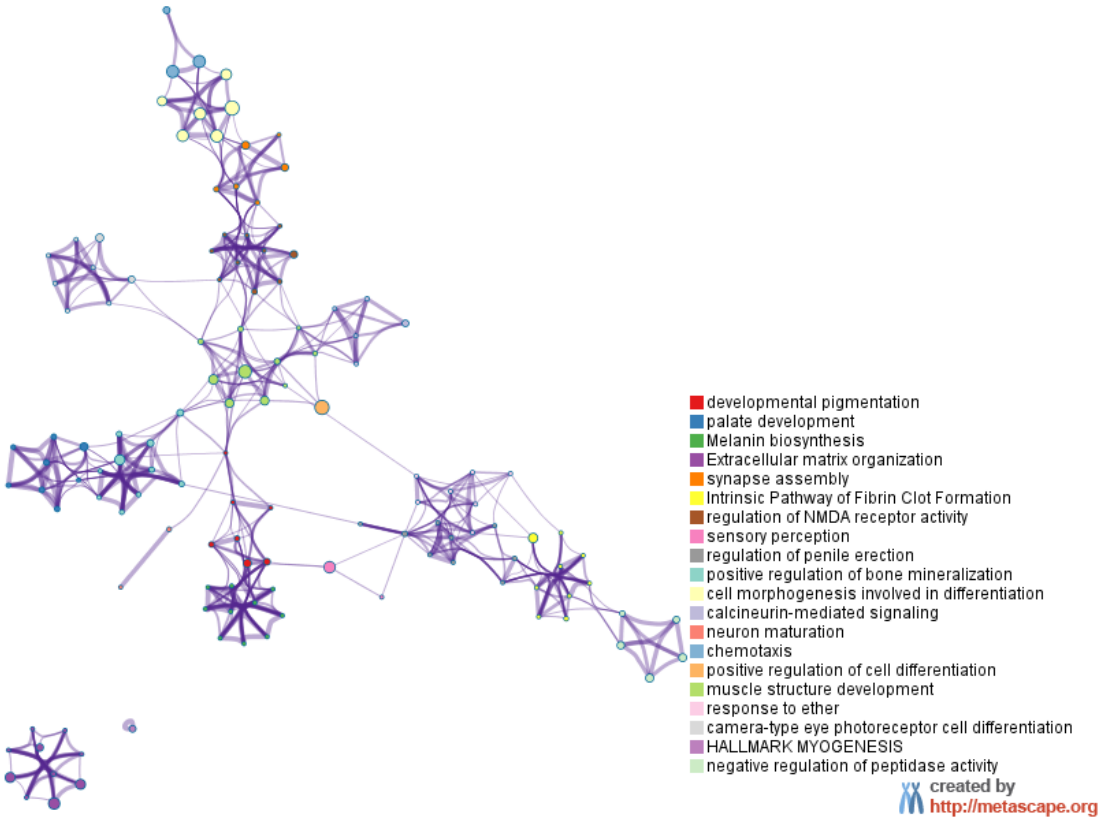

Figure S10. Enrichment network of the 222 genes that are down-regulated in PD-L1$_{CON}$ cell lines. Related to Figure 3. Representative terms from this the GO cluster analysis were converted into a network layout. Each term is represented by a circle node, where the size is proportional to the number of input genes that fall into the particular term, and the color represents its cluster identity (i.e., nodes of the same color belong to the same cluster). Terms with a similarity score > 0.3 are linked by an edge (the thickness of the edge represents the similarity score). The network is visualized with Cytoscape with the default layout. This analysis was performed using Metascape (http://metascape.org/gp/index.html#/main/step1).

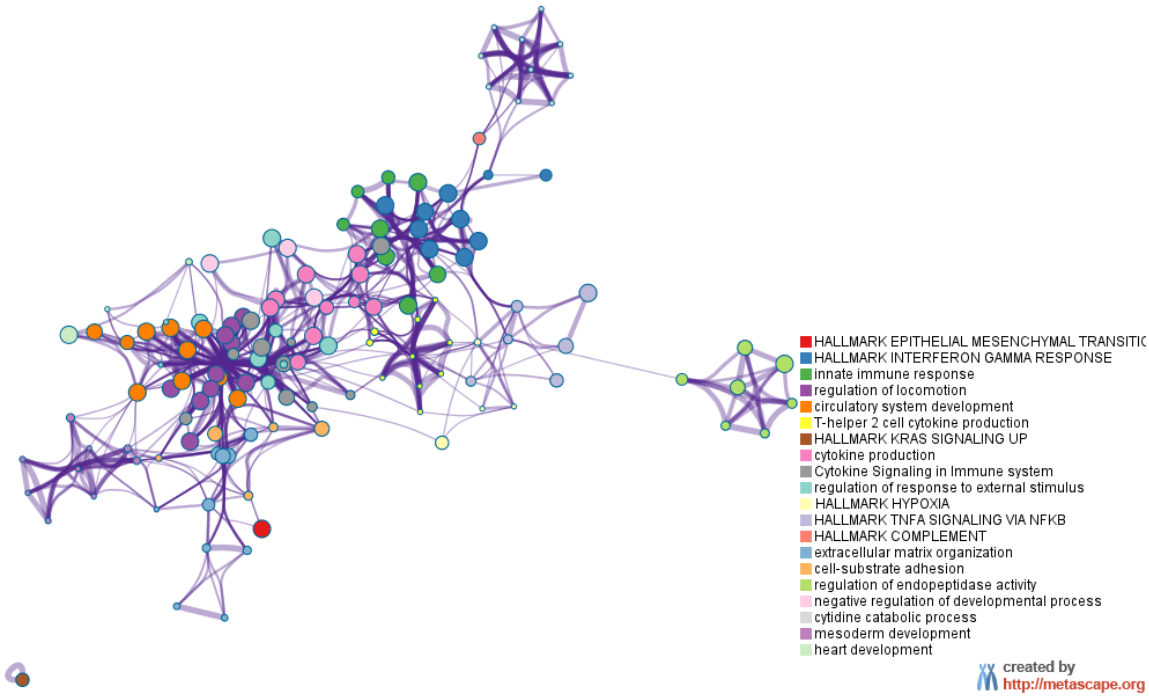

Figure S11. Enrichment network of the 286 genes that are up-regulated in PD-L1$_{CON}$ cell lines. Related to Figure 3. Representative terms from this the GO cluster analysis were converted into a network layout. Each term is represented by a circle node, where the size is proportional to the number of input genes that fall into the particular term, and the color represents its cluster identity (i.e., nodes of the same color belong to the same cluster). Terms with a similarity score > 0.3 are linked by an edge (the thickness of the edge represents the similarity score). The network is visualized with Cytoscape with the default layout. This analysis was performed using Metascape (http://metascape.org/gp/index.html#/main/step1).

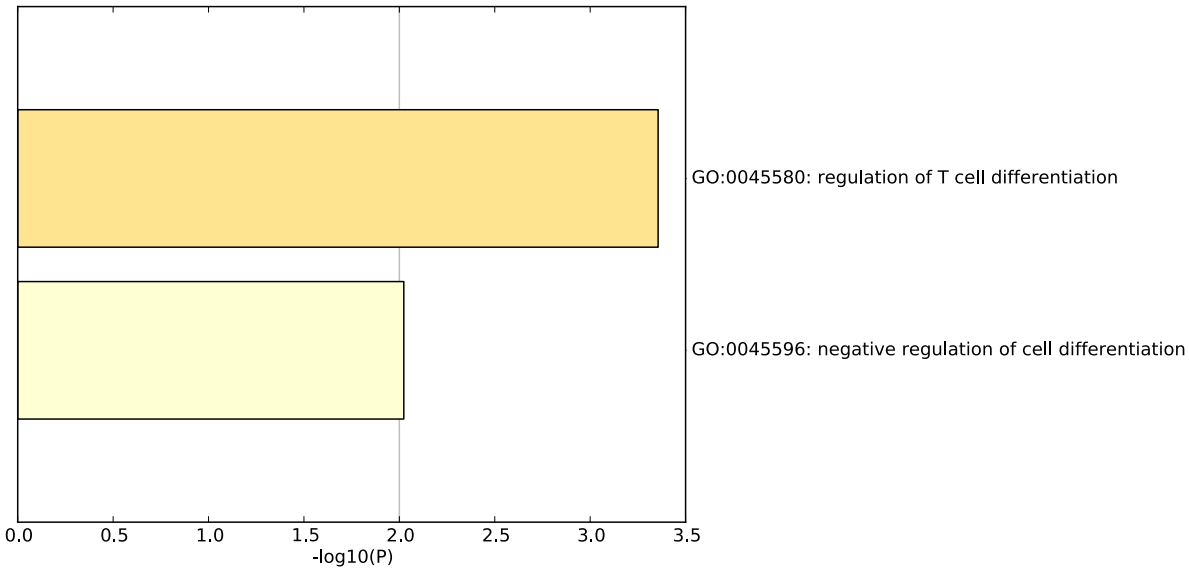

Figure S12. Enriched GO terms relative to the 58 genes that were very highly up-regulated in PD-L1$_{CON}$ cell lines. Related to Figure 3. The x-axis represents –log 10 of the *P*-value. This analysis was performed using Metascape (http://metascape.org/gp/index.html#/main/step1).

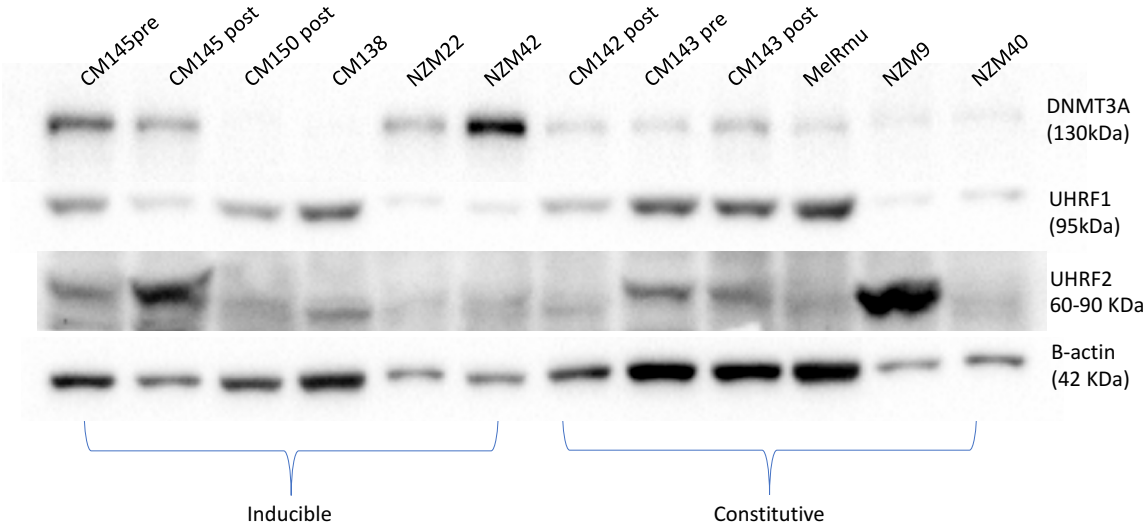

Figure S13. Western blot analysis of DNMT3A, UHRF1 and UHRF2 for PD-L1$_{IND}$ and PD-L1$_{CON}$ groups. Related to Figure 4. Western blots of cell lysates were performed with DNMT3A, UHRF1 and UHRF2 antibodies using a beta-actin antibody as a loading control; representative blots are shown.

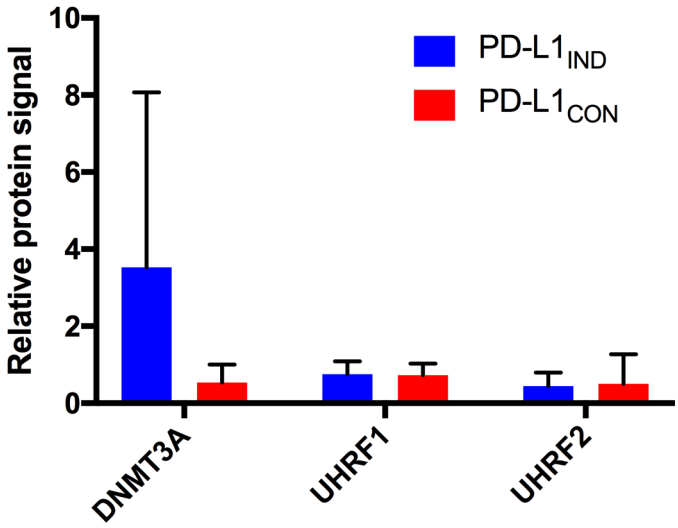

Figure S14. Quantification of DNMT3A, UHRF1 and UHRF2 protein levels for PD-L1$_{IND}$ and PD-L1$_{CON}$ groups. Related to Figure 4. Protein levels of DNMT3A, UHRF1 and UHRF2 were normalized against actin and are shown as mean ± SD for the PD-L1$_{IND}$ (n=6) and PD-L1$_{CON}$ (n=6) groups run in duplicate.

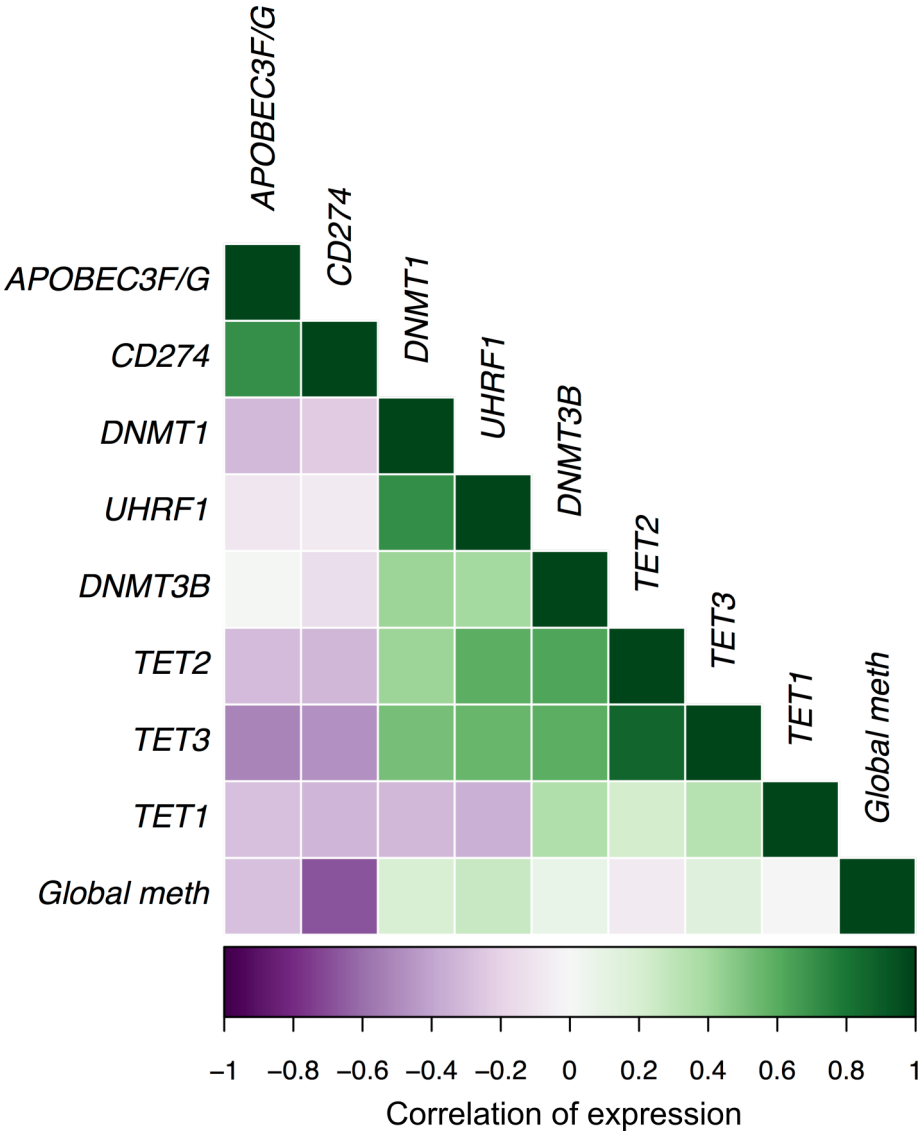

Figure S15. Relationship of methylation regulator genes with PD-L1 expression and global methylation levels. Related to Figure 4. Correlogram showing cross-correlation of major methylation regulator genes with *CD274* expression and global RRBS methylome in the analysed PD-L1$_{IND}$ and PD-L1$_{CON}$ cell lines.

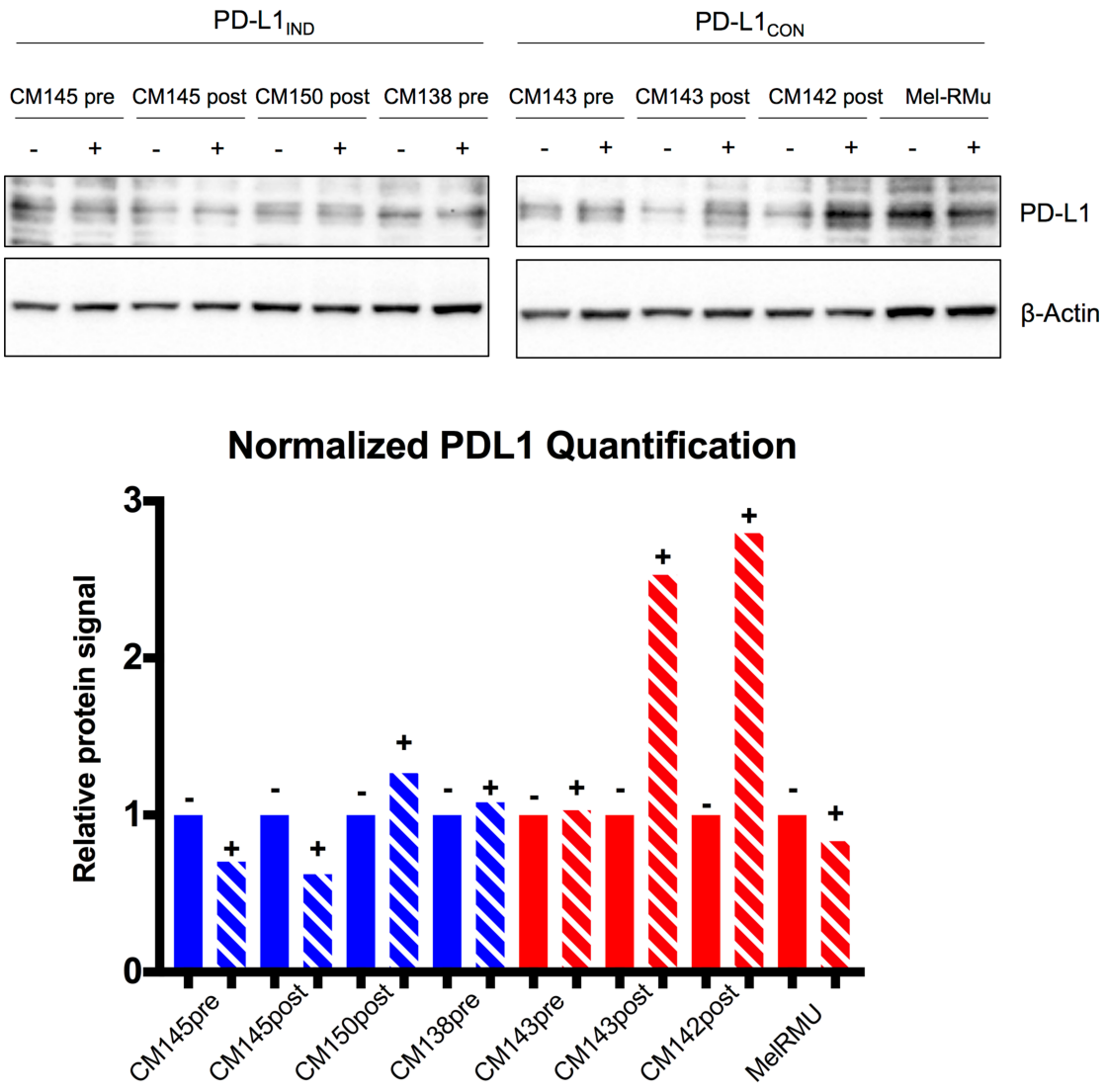

Figure S16. Total protein expression of PD-L1 for PD-L1$_{IND}$ and PD-L1$_{CON}$ groups with vs without decitabine treatment (100nM, 6 days). Related to Figure 6. Western blots of cell lysates were performed with a PD-L1 antibody using a beta-actin antibody as a loading control; representative blots are shown. Protein levels of PD-L1 were normalized against actin and are shown relative to untreated cells. "-" = without decitabine and "+" = with decitabine. All samples were done at least twice. Insufficient samples available for NZM cell lines, therefore these are not shown here.

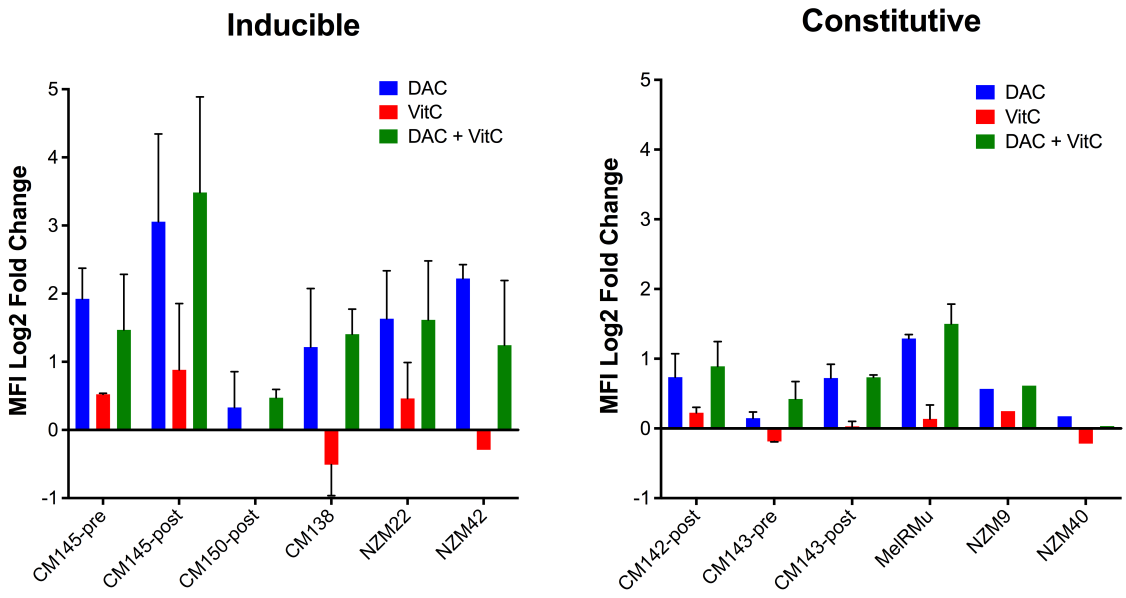

Figure S17. Flow cytometry analysis of PD-L1 cell surface expression upon single and combination treatment of DNMTi (demethylation) and vitamin C in PD-L1$_{IND}$ and PD-L1$_{CON}$ cell lines. Related to Figure 6. Flow cytometry analysis for PD-L1$_{IND}$ (A) and PD-L1$_{CON}$ (B) cell lines were performed at day 6 for all 3 treatment groups of decitabine (DAC), vitamin C (VitC) and decitabine with vitamin C (DAC + VitC). Decitabine (DNMTi; 0.5uM) and mock treatment (DMSO) were performed for 3 daily consecutive days while vitamin C treatment was done for 6 daily consecutive days. PD-L1 expression changes were calculated using medium fluorescence intensities (MFI) using the same formula previously mentioned (see Transparent Methods). Error bars represent SE of two technical replicates.

Supplemental Tables:

Table S1. Percentage of PD-L1 positive cell in the analysed cell lines (from FACS data). Related to Figure 1.

Cell line name	$PD\text{-}L1_{IND}$ or $PD\text{-}L1_{CON}$ Status	% of PD-L1 positive cells	Mutation status
CM145-pre	Inducible	2.22	BRAF V600E
CM145-post	Inducible	1.18	BRAF V600E
CM150-post	Inducible	1.00	BRAF V600E
CM138	Inducible	2.95	BRAF V600E
NZM22	Inducible	6.79	TP53 241S/T/W
NZM42	Inducible	0.82	NRAS Q61K
CM142-post	Constitutive	88.53	BRAF V600E
CM143-pre	Constitutive	83.55	BRAF V600E
CM143-post	Constitutive	98.61	BRAF V600E
MEL-RMU	Constitutive	41.60	BRAF V600E
NZM9	Constitutive	99.07	TP53 179C/T, CDKN2A del
NZM40	Constitutive	98.99	NRAS Q61H, TP53 del249-253, PIK3CA H1047R

Table S2. Details of sequenced reads and mapping for the PD-L1IND and PD-L1CON cell lines. Related to Figure 2.

Cell line name	$PD\text{-}L1_{IND}$ or $PD\text{-}L1_{CON}$ Status	Number of sequenced reads	% of Unique bisulfite mapping
CM145-pre	Inducible	49593852	64.10%
CM145-post	Inducible	17151339	60.90%
CM150-post	Inducible	53768394	64.70%
CM138	Inducible	21470763	61.40%
NZM22	Inducible	42521971	67.10%
NZM42	Inducible	39082074	62.60%
CM142-post	Constitutive	71051964	64.50%
CM143-pre	Constitutive	35395530	67.50%
CM143-post	Constitutive	34604864	67.20%
MEL-RMU	Constitutive	73919898	68.00%
NZM9	Constitutive	43655388	61.80%
NZM40	Constitutive	52776715	64.20%

Table S3. Global methylation profiles in different genomic elements in the PD-L1IND and PD-L1CON cell lines. Related to Figure 2 (see Figure 2A in the main manuscript and the description)**.**

Genome Elements	$PD\text{-}L1_{IND}$		$PD\text{-}L1_{CON}$	
	Median	**Mean**	**Median**	**Mean**
Genome-wide	0.63	0.54	0.47	0.48
Promoter	0.06	0.22	0.07	0.22
Intron	0.71	0.57	0.59	0.54
Intron/Exon	0.6	0.5	0.51	0.49
Exon	0.47	0.47	0.43	0.47
Intergenic	0.67	0.59	0.48	0.49

Table S4. Comparison of DNA methylation profiles in different repeat elements for PD-L1IND and PD-L1CON cell lines. Related to Figure 2 (see Figure 2B-2E in the main manuscript and the description).

	Number of	$PD\text{-}L1_{IND}$		$PD\text{-}L1_{CON}$	
	Analysed Fragments	**median**	**mean**	**median**	**mean**
LINEs					
L1	4851	0.72	0.67	0.53	0.54
L2	4225	0.75	0.67	0.64	0.59
Satellite elements					
Telomere	214	0.66	0.6	0.55	0.55
Satellite	305	0.57	0.53	0.39	0.43
Centromere	598	0.58	0.57	0.46	0.48
SINEs					
Alu	97416	0.88	0.79	0.79	0.69
MIR	5619	0.71	0.63	0.6	0.56
LTRs					
ERV1	11587	0.79	0.72	0.6	0.58
ERVK	875	0.68	0.63	0.52	0.52
ERVL	1984	0.72	0.66	0.57	0.55
ERVL-MalR	2603	0.73	0.68	0.6	0.58

Table S5. Details of DMFs that exhibit a significant positive or negative association of methylation and concomitant differential expression with either PD-L1IND or PD-L1CON cell line groups. Related to Figure 4. Instances where multiple DMFs are associated with a single gene are also shown here.

DMF loci (GRCh37)	PD-L1$_{IND}$ meth	PD-L1$_{CON}$ meth	Diffmeth adjusted P value (FDR 5%)	Overlapping gene	Predicted regulatory feature, target gene(s), Genehancer score	PD-L1$_{IND}$ FPKM	PD-L1$_{CON}$ FPKM	Cuffdiff adjusted P value (FDR 5%)	Spearman correlation of DMF methylation vs target gene[1] expression
chr2:80136765-80136845	0.93	0.23	4.59E-04	*CTNNA2* Exon	-	3.29	0.05	5.35E-03	0.87
chr2:152780685-152780752	0.72	0.13	1.53E-02	*CACNB4* Intron	-	0.06	0.5	1.34E-02	0.07
chr2:171353982-171354051	0.83	0.26	4.07E-02	*MYO3B* Intron	-	0.31	0.01	5.35E-03	0.67
chr3:430086-430153	0.62	0.15	1.61E-03	*CHL1* Intron	-	10.18	0.04	5.35E-03	0.77
chr3:12368678-12368759	0.1	0.89	3.16E-02	*PPARG* Intron	Enhancer: *PPARG* (35.15), *SYN2* (19.35), *TIMP4* (10.18)	0.71	13.97	5.35E-03	0.75
chr3:37540164-37540228	0.86	0.27	2.59E-02	*ITGA9* Intron	-	8.45	0.07	1.09E-02	0.75
chr3:62692712-62692781	0.79	0.23	2.46E-02	*CADPS* Intron	-	4.1	0.23	2.24E-02	0.68
chr3:123120672-123120773	0.74	0.23	3.30E-02	*ADCY5* Intron	-	1.06	0.12	1.34E-02	0.18
chr4:79152150-79152200	0.96	0.24	1.63E-02	*FRAS1* Intron	-	1.74	0.05	5.35E-03	0.82
chr5:155328178-155328245	0.78	0.09	2.74E-02	*SGCD* Intron	-	19.42	0.01	2.38E-02	0.75
chr5:155363892-155363936	0.78	0.12	4.64E-02	*SGCD* Intron	-	19.42	0.01	2.38E-02	0.8
chr5:155404827-155404930	0.81	0.06	6.42E-03	*SGCD* Intron	-	19.42	0.01	2.38E-02	0.77
chr5:155423509-155423595	0.8	0.07	3.10E-02	*SGCD* Intron	-	19.42	0.01	2.38E-02	0.79
chr5:155559547-155559638	0.88	0.12	1.18E-03	*SGCD* Intron	-	19.42	0.01	2.38E-02	0.78
chr5:155675386-155675452	0.89	0.12	3.38E-05	*SGCD* Intron	-	19.42	0.01	2.38E-02	0.8
chr5:155756883-155756950	0.97	0.28	2.20E-02	*SGCD* Intron	Enhancer: *SGCD* (9.64)	19.42	0.01	2.38E-02	0.65
chr5:156028793-156028853	0.96	0.29	7.01E-03	*SGCD* Intron	-	19.42	0.01	2.38E-02	0.89
chr5:156046196-156046328	0.94	0.24	2.11E-03	*SGCD* Intron	-	19.42	0.01	2.38E-02	0.89
chr5:156179564-156179698	0.94	0.23	4.05E-04	*SGCD* Intron	-	19.42	0.01	2.38E-02	0.77
chr5:160111896-160112036	0.83	0.28	3.27E-02	*ATP10B* Intron	Enhancer: *ATP10B* (10.72)	9.32	0.04	5.35E-03	0.7
chr5:160114492-160114627	0.83	0.19	2.20E-02	*ATP10B* Intron	-	9.32	0.04	5.35E-03	0.87
chr5:160201234-160201323	0.9	0.23	8.11E-03	*ATP10B* Intron	-	9.32	0.04	5.35E-03	0.83
chr5:172204336-172204415	0.94	0.31	2.59E-03	Intergenic	Enhancer: *DUSP1* (41.11), *CREBRF* (34.7), *KLF3P1* (20.24), *ERGIC*	10.43	97.48	5.35E-03	-0.65
chr6:401453-401500	0.83	0.42	2.04E-02	*IRF4* Exon	miRNA target site (hsa-miR-205-5p)	12.84	0.08	1.09E-02	0.68
chr7:95583327-95583402	0.86	0.25	1.87E-02	*DYNC1I1* Intron	-	9.84	0.87	1.73E-02	0.21
chr7:151454112-151454226	0.14	0.74	4.55E-02	*PRKAG2* Intron	Enhancer: *PRKAG2* (18.77), *CRYGN* (9.74), *AOC1* (5.42), *SMARCD*	3.54	27.87	5.35E-03	0.68
chr8:95648544-95648611	0.88	0.53	1.69E-02	*ESRP1* Promoter	-	14.51	0.17	5.35E-03	0.73
chr8:120983123-120983191	0.83	0.45	4.23E-02	*DEPTOR* Intron	Enhancer, *COL14A1*, (11.4), *DEPTOR* (25.26), *TAF2* (15.92), *DSCC*	4.07	0.44	2.38E-02	0.29
chr8:121137204-121137324	0.85	0.34	4.87E-02	*COL14A1* Intron	-	4.07	0.44	2.38E-02	0.35
chr8:121206338-121206403	0.83	0.29	3.05E-02	*COL14A1* Intron	-	4.07	0.44	2.38E-02	0.37
chr8:143546627-143546726	0.88	0.32	3.91E-02	*BAI1* Intron	TF binding: *BAI1*	12.44	0.22	5.35E-03	0.8
chr8:143596462-143596531	0.9	0.34	4.91E-02	*BAI1* Intron	-	12.44	0.22	5.35E-03	0.9
chr9:90237682-90237749	0.95	0.45	3.75E-02	*DAPK1* Intron	-	8.03	0.25	5.35E-03	0.71
chr9:90238526-90238632	0.9	0.24	3.06E-03	*DAPK1* Intron	-	8.03	0.25	5.35E-03	0.83
chr9:90292483-90292556	0.85	0.19	2.56E-03	*DAPK1* Intron	-	8.03	0.25	5.35E-03	0.85
chr9:130687304-130687414	0.64	0.91	1.53E-02	*PIP5KL1* Intron/Exon	-	0.48	3.24	5.35E-03	0.76
chr9:130764274-130764342	0.82	0.23	2.59E-03	Intergenic	Enhancer: *PIP5KL1* (15.46), *FAM102A* (12.71), *DPM2* (12.12), *SLC.*	0.48	3.24	5.35E-03	-0.66
chr10:108522243-108522310	0.9	0.18	6.09E-03	*SORCS1* Intron	-	9.27	0.42	2.24E-02	0.74
chr10:108527407-108527543	0.72	0.09	4.65E-02	*SORCS1* Intron	-	9.27	0.42	2.24E-02	0.83
chr10:108554421-108554554	0.77	0.11	2.50E-02	*SORCS1* Intron	-	9.27	0.42	2.24E-02	0.9
chr10:108627203-108627335	0.85	0.16	3.87E-02	*SORCS1* Intron	-	9.27	0.42	2.24E-02	0.81
chr10:108638764-108638831	0.88	0.16	1.77E-02	*SORCS1* Intron	-	9.27	0.42	2.24E-02	0.94
chr10:108689896-108689963	0.75	0.27	4.92E-02	*SORCS1* Intron	-	9.27	0.42	2.24E-02	0.59
chr10:108873305-108873371	0.96	0.25	5.31E-03	*SORCS1* Intron	-	9.27	0.42	2.24E-02	0.68
chr10:124275587-124275651	0.73	0.24	1.76E-02	Intergenic	Enhancer: *DMBT1* (0.24)	0.02	1.14	4.32E-02	-0.69
chr11:17452263-17452344	0.9	0.41	3.26E-02	*ABCC8* Intron	-	0.57	0.05	5.35E-03	0.69
chr11:17796384-17796481	0.55	0.19	4.87E-02	*KCNC1* Intron	-	2.17	0.11	3.80E-02	0.78
chr11:21544483-21544550	0.76	0.05	1.39E-03	*NELL1* Intron	-	1.37	0.04	1.09E-02	0.53
chr11:21544551-21544687	0.71	0.04	2.36E-02	*NELL1* Intron	-	1.37	0.04	1.09E-02	0.81
chr13:24785859-24785904	0.97	0.62	2.21E-03	*SPATA13* Intron	-	12.09	2.91	5.35E-03	0.84

chr13:113734978-113735030	0.9	0.38	4.53E-02	*MCF2L* Intron	-	40.78	4.02	2.10E-02	0.82
chr13:113743774-113743822	0.72	0.34	3.05E-02	*MCF2L* Intron	-	40.78	4.02	2.10E-02	0.8
chr13:114560770-114560828	0.24	0.83	2.53E-02	*GAS6* Intron	Enhancer: *GAS6* (7.24), *GAS6-AS1* (6.28)	8.86	46.94	1.73E-02	0.64
chr14:92336674-92336742	0.86	0.29	2.25E-03	*FBLN5* Intron/Exon	Enhancer, *FBLN5* (16.76), *TC2N* (9.43), *CATSPERB* (8.39)	4.2	1	3.94E-01	0.34
chr15:28098835-28098919	0.84	0.42	2.24E-02	*OCA2* Intron	-	15.47	0.19	4.41E-02	0.5
chr15:28211953-28212063	0.72	0.26	2.22E-02	*OCA2* Intron/Exon	-	15.47	0.19	4.41E-02	0.27
chr15:28249365-28249463	0.62	0.17	2.30E-02	*OCA2* Intron	-	15.47	0.19	4.41E-02	0.27
chr15:28252732-28252799	0.87	0.24	5.31E-03	*OCA2* Intron	-	15.47	0.19	4.41E-02	0.37
chr15:28300866-28300920	0.41	0.05	4.01E-02	*OCA2* Intron	-	15.47	0.19	4.41E-02	0.38
chr15:100694107-100694241	0.92	0.32	4.44E-02	*ADAMTS17* Intron	-	4.2	0.17	5.35E-03	0.79
chr15:100709864-100709979	0.92	0.6	2.90E-02	*ADAMTS17* Intron	-	4.2	0.17	5.35E-03	0.9
chr15:100710120-100710181	0.77	0.13	5.85E-03	*ADAMTS17* Intron	-	4.2	0.17	5.35E-03	0.86
chr15:100773984-100774069	0.96	0.25	1.53E-02	*ADAMTS17* Intron	-	4.2	0.17	5.35E-03	0.81
chr15:101977557-101977611	0.78	0.21	4.40E-02	*PCSK6* Intron	-	6.18	0.67	5.35E-03	0.83
chr16:1029727-1029802	0.87	0.23	4.63E-02	*SOX8* Promoter	-	31.78	0.17	1.09E-02	0.73
chr17:71546113-71546180	0.76	0.22	4.88E-02	*SDK2* Intron	TF binding: *SDK2*	3.19	0.26	5.35E-03	0.79
chr17:71593122-71593178	0.89	0.26	1.01E-02	*SDK2* Intron	-	3.19	0.26	5.35E-03	0.65
chr17:71593179-71593332	0.76	0.24	1.53E-02	*SDK2* Intron	-	3.19	0.26	5.35E-03	0.83
chr17:71607953-71608022	0.87	0.23	4.07E-02	*SDK2* Intron	Enhancer: *SDK2* (18.32)	3.19	0.26	5.35E-03	0.78
chr18:4147291-4147358	0.81	0.12	9.81E-03	*DLGAP1* Intron	-	2.54	0.04	5.35E-03	0.47
chr18:47498335-47498444	0.83	0.25	5.00E-02	*MYO5B* Intron	-	0.35	1.05	6.37E-01	0.21
chr18:74241157-74241268	0.9	0.37	4.92E-02	Intergenic	Enhancer: *ZNF516* (5.24)	7.75	1.9	3.92E-02	0.72
chr19:5909678-5909795	0.25	0.93	1.01E-02	*VMAC* Exon	Enhancer: *CAPS* (33.18), *NDUFA11* (13.52), *VMAC* (0.4)	127.98	2.43	5.35E-03	-0.75
chr19:5910435-5910563	0.1	0.8	2.80E-02	*CAPS* Promoter	-	127.98	2.43	5.35E-03	-0.85

Table S7. Primer Sequences for RT PCR analysis for the 9 HERV genes. Related to Figure 5.

Gene names	Forward sequence	Reverse sequence
MLTA10	TCTCACAATCCTGGAGGCTG	GACCAAGAAGCAAGCCCTCA
MLT1B	TGCCTGTCTCCAAACACAGT	TACGGGCTGAGCTTGAGTTG
MER21C	GGAGCTTCCTGATTGGCAGA	ATGTAGGGTGGCAAGCACTG
ERVL	ATATCCTGCCTGGATGGGGT	GAGCTTCTTAGTCCTCCTGTGT
MLT1C49	TATTGCCGTACTGTGGGCTG	TGGAACAGAGCCCTTCCTTG
MLT1C627	TGTGTCCTCCCCCTTCTCTT	GCCTGTGGATGTGCCCTTAT
MER4D	CCCTAAAGAGGCAGGACACC	TCAAGCAATCGTCAACCAGA
MER57B1	CCTCCTGAGCCAGAGTAGGT	ACCAGTCTGGCTGTTTCTGT
MTL2B4	GGAGAAGCTGATGGTGCAGA	ACCAACCTTCCCAAGCAAGA
SRP14	ACGGAGCTGACCAGACTTTTC	TGGTTCGACCGTCATACTTCTT
RPL27	TGGCTGGAATTGACCGCTAC	CCTTGTGGGCATTAGGTGATTG

Transparent Methods:

Ethics statement: The generation of the cell lines was approved by the Hunter and New England Research Ethics Committee, Australia.

Characterisation of the PD-L1 cell lines: Cell cultures were established as described previously from patients entered into the Roche "BRIM II" phase II study of vemurafenib in patients who had failed previous treatment (Franco et al., 2001). The patient lines were established prior to, and during relapse from treatment with vemurafenib, labelled "pre" and "post" respectively and as described elsewhere (Lai et al., 2012). Cells were cultured in Dulbecco's modified Eagle medium (DMEM) containing 10% fetal calf serum (FCS) (AusGeneX, Brisbane, Australia). All cell lines were tested for mutations using the OncoCARTA and or MelaCARTA panel and contained melanoma associated mutations. In addition, we also used the Geneprint 10 system (Promega, Madison, WI) for authentication and matching of the cell lines.

FACS analysis: The constitutive and inducible status of these cell lines was determined by FACS analysis. The PD-L1 positive percentage was determined using flow cytometry by setting an expression threshold on the isotype control. The gate on the isotype control was set to allow approximately 0.5% of the events to be above the threshold. Subsequently, these gates were applied to the PD-L1 stained samples to determine the PD-L1 positive percentage. All the analysed melanoma cell lines were stained with anti-PD-L1 (PE) and the isotype control antibody. An expression level of at least fivefold higher than the isotype control was considered as "constitutive" expression of PD-L1 (see FACS analysis figures in Supplemental Figure S1-S2).

Interferon blocking experiment: PD-L1$_{CON}$ cell lines CM143-pre and CM143-post were treated with blocking antibodies against interferon a receptor 2 (IFNAR2) (clone MMHAR-2, PBL Assay Science, Piscataway, NJ, 10mg/ml), IFNgR1 (clone GIR20s8, R&D Systems, Minneapolis, MN, 5mg/ml), or IFNg (clone NIB42, Beckton Dickinson, Franklin Lakes, NJ, 100ng/ml) in the absence or presence of 10^4 U IFNa2A (Stemcell Technologies, Vancouver, Canada) or 100ng/ml IFN-g (R&D Systems, Minneapolis, MN), as appropriate. PD-L1 expression was measured by flow cytometry on day 3.

RRBS library preparation and sequencing: We used reduced representation bisulfite sequencing (RRBS) to map promoter and gene body DNA methylation as described previously (Chatterjee et al., 2016a; Chatterjee et al., 2013; Chatterjee et al., 2012a; Chatterjee et al., 2014; Chatterjee et al., 2015b). Briefly, genomic DNA was digested with MspI followed by end-repair and ligation of sequencing adaptors. The fragments were size selected and bisulfite-converted prior to a PCR amplification step. The quality and size distribution of the libraries was determined using a bioanalyser and four libraries were sequenced per flow cell lane of an Illumina HiSeq2500 machine (100 bp reads, single-ended).

DNA methylation data analysis: The quality check and processing of the sequenced RRBS reads was performed using in-house developed bioinformatics tools as previously described (Chatterjee et al., 2012b; Stockwell et al., 2014). The Bismark tool (Krueger and Andrews, 2011) was used to align the processed sequence reads to the reference human genome (GRCh37). We applied stringent mapping criteria by

allowing only one mismatch (default = 2) in the seed (i.e., in the first 28 bp of the sequenced reads). After filtering for low quality sequences, we obtained > 60% unique alignment for all the PD-L1$_{CON}$ and PD-L1$_{IND}$ RRBS libraries, respectively. The median non-CpG DNA methylation was 1.95% and 2.45% in the PD-L1$_{CON}$ and PD-L1$_{IND}$ libraries, respectively (as measured by Bismark alignment), indicating effective bisulfite conversion and low levels of true non-CpG methylation.

The distribution and level of CpG DNA methylation (on a scale of 0–1) was determined, using MspI fragments (40–220 bp) as the unit of analysis rather than individual CpG sites or a tiled window approach, as previously described (Chatterjee et al., 2016b; Chatterjee et al., 2017; Chatterjee et al., 2015b; Chatterjee et al., 2016c). Differential methylation analysis was performed with an in-house Differential Methylation Analysis Pipeline (DMAP), which contains two main programmes (diffmeth and identgenloc) (Stockwell et al., 2014). Briefly, we applied an F statistic (ANOVA test) on fragments that had high quality methylation information (at least two CpG sites covered by 10 or more sequenced reads, -F 2 -t 10 switch in the diffmeth program of the DMAP tool) in at least 3 cell lines in each group, and identified regions showing the largest methylation difference and significant *P*-values. We applied a false discovery rate of 5% on the analysed fragments (at an alpha level = 0.05) to filter for significant fragments. We further filtered this list and obtained fragments with 0.25 (i.e., 25%) of higher methylation difference (mean methylation on fragments) between the PD-L1$_{CON}$ and PD-L1$_{IND}$ groups.

RNA isolation and construction of RNA-Seq libraries: RNA was extracted from cell lines using an RNeasy Plus mini prep kit (QIAGEN, Limburg, Netherlands), and quantified using Nanodrop (Thermo Scientific, Wilmington, DE) as previously described (Chatterjee et al., 2015a; Leichter et al., 2015). RNA quality was assessed using Bioanalyser analysis of RNA integrity number (RIN) (Agilent, USA). RNA libraries were constructed using 1µg of total RNA with a TruSeq stranded mRNA Sample Preparation kit (Illumina) following the manufacturer's protocol. Briefly, poly-A containing mRNA was purified using oligo-dT magnetic beads. Next, RNA fragments were reverse transcribed using random primers and reverse transcriptase and first strand cDNA was synthesized. Following this, second strand cDNA was synthesized, and the cDNA was blunt-ended, which was followed by 'A' tailing and adaptor ligation. The adaptor ligated cDNA was amplified by PCR for sequencing.

Analysis of transcriptomic data: RNA was sequenced on an Illumina HiSeq 2500 sequencer (Illumina, USA) with paired-end, 101-bp runs producing raw fastq files. The RNA-seq reads were adaptor trimmed using the cleanadaptors tool (Chatterjee et al., 2012b) and mapped to the human genome (assembly GRCh37) using TopHat2 (Kim et al., 2013). Transcripts were assembled and normalized gene expression levels were expressed in FPKM (Fragments Per Kilo base per Million) values as generated by cuffquant and cuffnorm programmes (Trapnell et al., 2012). Assembly of transcripts and generation of the FPKM values was performed with the option ''–frag-bias- correct'' and ''–multi-read-correct'' to improve sensitivity of transcript detection (Roberts et al., 2011). We identified 557 genes that were significantly differentially expressed (DEG) between PD-L1$_{IND}$ and PD-L1$_{CON}$ cell lines (P-value <0.05, FDR corrected). We further filtered this list based on fold-expression change and selected the genes that showed $\log_2$ fold change of mean FPKM (fragment per kilobase per million read) ≥ 2, resulting in 508 DEGs (analysed with cuffdiff

(Trapnell et al., 2012)). The list of epigenetic regulator genes was obtained from EpiFactors database (Medvedeva et al., 2015). Pathway analysis on DEGs was performed using Metascape (METASCAPE.ORG).

TCGA data analysis and deconvolution of based on TIL and PD-L1 expression: TCGA Firehose level 3 data for skin cutaneous melanoma was downloaded using an R package (Samur, 2014). Clinical details, methylation 450k and RNAseqV2 with run date "20151101" were selected for download. The RNA-Seq data are RSEM normalised values with expected counts for each gene. Samples were filtered to 469 samples after retaining only those samples with information on all three of the following; clinical details, methylation 450k and RNA-seq data. RNA-seq data was used to generate three values that infered the quantity of CD8 TILs using computational tools including CiberSort (Newman et al., 2015) MCPcounter (Becht et al., 2016) and xCell (Aran et al., 2017). Methylation 450k data were used to generate the meTIL (methylation TIL) score. This was calculated with beta-values from five CpG probes using the formula provided by Jeschke et al (Jeschke et al., 2017). To obtain the average TIL score from these four variables, first all zero CD8 values produced from CiberSort, MCPcounter and xCell were converted to half of the smallest value in that corresponding variable. These three variables were logarithmically transformed. All four variables were scaled to generate Z-scores by subtracting the mean and dividing by the standard deviation. The average TIL score was then calculated for each sample using the arithmetic mean. The average TIL-score and PD-L1 mRNA values were used to generate four groups from 469 samples according to high and low presence of TILs and PD-L1 expression. First, samples were split according to high and low TIL-score values using the median as a cut-off threshold. Samples were then split again using the median PD-L1 mRNA expression levels as the cut-off. Groups 1 and 2 represent the inducible and constitutive patient groups (see Supplemental Figure S9-S10 for their TIL and PD-L1 levels).

qPCR analysis of HERV genes: Total RNA was extracted using the RNeasy Mini Kit (Qiagen) and reverse transcription was performed using the High-Capacity cDNA Reverse Transcription Kit (ThermoFisher). RT-PCR was run on the Light Cycler 480 (Roche) using SYBR green (SYBR Premix Ex Taq II, Takara). Primers were acquired from Roulois et al (Roulois 2015) and are listed in Supplemental Table S7. Gene expressions were normalised to house-keeping genes RPL27 and SPR14 and analysis was done using the qbaseplus software (Biogazelle).

Western blot analysis: Cell pellets were washed in ice-cold PBS and lysed using RIPA buffer containing a protease inhibitor cocktail. After centrifugation, supernatants were collected and total protein quantified using the Biorad DC protein assay. 20-40µg of total protein was electrophoresed on 8-12% SDS-PAGE gels and transferred onto nitrocellulose membranes. Membranes were blocked and incubated overnight in one of the following primary antibodies: PD-L1 (#AF156, R&D Systems), DNMT3A (#3598, Cell Signalling), UHRF1 (#12387, Cell Signalling), UHRF2 (#PA5-40969, Thermo Fisher), ß-actin (#A2228, Sigma) and α-tubulin (#T5168, Sigma). Following incubation in the appropriate HRP-conjugated secondary antibodies, chemiluminescent imaging was performed on a Chemidoc imaging system. Western blot images were analysed using LI-COR Image Studio software.

Data availability: DNA methylation and transcriptomic data for PD-$L1_{CON}$ and PD-$L1_{IND}$ cell lines are available at Database: NCBI GEO, accession number GSE107622.

DNMTi treatment of PD-L1 cell lines and data analysis: All twelve cell lines were treated with decitabine (500nM; Sigma Aldrich, DNMTi treatment) or DMSO (Sigma Aldrich), while changing the media containing fresh drug or vehicle daily, for three consecutive days. Subsequently, cells were grown in fresh media (without drug) for an additional three days. At day six cells were harvested for flow cytometry analysis. An independent biological replicate study was carried out using the same experimental conditions, and treated with 100nM decitabine, generated essentially the same results. Western blots were performed to confirm PD-L1 protein levels upon demethylation (Supplemental Figure S11). Flow cytometry analysis was performed as described above. Changes of PD-L1 expression between decitabine-treated and control were calculated using medium fluorescence intensities (MFI) and the formula: $\log_2([(MFI_{antibody,\ treated})-(MFI_{isotype,\ treated})]/\ [(MFI_{antibody,\ mock})-(MFI_{isotype,\ mock})])$ (Wrangle et al., 2013).

Supplemental References:

Aran, D., Hu, Z., and Butte, A.J. (2017). xCell: digitally portraying the tissue cellular heterogeneity landscape. Genome Biol *18*, 220.

Becht, E., Giraldo, N.A., Lacroix, L., Buttard, B., Elarouci, N., Petitprez, F., Selves, J., Laurent-Puig, P., Sautes-Fridman, C., Fridman, W.H.*, et al.* (2016). Estimating the population abundance of tissue-infiltrating immune and stromal cell populations using gene expression. Genome Biol *17*, 218.

Chatterjee, A., Lagisz, M., Rodger, E.J., Zhen, L., Stockwell, P.A., Duncan, E.J., Horsfield, J.A., Jeyakani, J., Mathavan, S., Ozaki, Y.*, et al.* (2016a). Sex differences in DNA methylation and expression in zebrafish brain: a test of an extended 'male sex drive' hypothesis. Gene *590*, 307-316.

Chatterjee, A., Leichter, A.L., Fan, V., Tsai, P., Purcell, R.V., Sullivan, M.J., and Eccles, M.R. (2015a). A cross comparison of technologies for the detection of microRNAs in clinical FFPE samples of hepatoblastoma patients. Sci Rep *5*, 10438.

Chatterjee, A., Macaulay, E.C., Rodger, E.J., Stockwell, P.A., Parry, M.F., Roberts, H.E., Slatter, T.L., Hung, N.A., Devenish, C.J., and Morison, I.M. (2016b). Placental Hypomethylation Is More Pronounced in Genomic Loci Devoid of Retroelements. G3 (Bethesda) *6*, 1911-1921.

Chatterjee, A., Ozaki, Y., Stockwell, P.A., Horsfield, J.A., Morison, I.M., and Nakagawa, S. (2013). Mapping the zebrafish brain methylome using reduced representation bisulfite sequencing. Epigenetics *8*, 979-989.

Chatterjee, A., Rodger, E.J., Stockwell, P.A., Weeks, R.J., and Morison, I.M. (2012a). Technical considerations for reduced representation bisulfite sequencing with multiplexed libraries. J Biomed Biotechnol *2012*, 741542.

Chatterjee, A., Stockwell, P.A., Ahn, A., Rodger, E.J., Leichter, A.L., and Eccles, M.R. (2017). Genome-wide methylation sequencing of paired primary and metastatic cell lines identifies common DNA methylation changes and a role for EBF3 as a candidate epigenetic driver of melanoma metastasis. Oncotarget *8*, 6085-6101.

Chatterjee, A., Stockwell, P.A., Horsfield, J.A., Morison, I.M., and Nakagawa, S. (2014). Base-resolution DNA methylation landscape of zebrafish brain and liver. Genom Data *2*, 342-344.

Chatterjee, A., Stockwell, P.A., Rodger, E.J., Duncan, E.J., Parry, M.F., Weeks, R.J., and Morison, I.M. (2015b). Genome-wide DNA methylation map of human

neutrophils reveals widespread inter-individual epigenetic variation. Sci Rep *5*, 17328.
Chatterjee, A., Stockwell, P.A., Rodger, E.J., and Morison, I.M. (2012b). Comparison of alignment software for genome-wide bisulphite sequence data. Nucleic Acids Res *40*, e79.
Chatterjee, A., Stockwell, P.A., Rodger, E.J., and Morison, I.M. (2016c). Genome-scale DNA methylome and transcriptome profiling of human neutrophils. Sci Data *3*, 160019.
Franco, A.V., Zhang, X.D., Van Berkel, E., Sanders, J.E., Zhang, X.Y., Thomas, W.D., Nguyen, T., and Hersey, P. (2001). The role of NF-kappa B in TNF-related apoptosis-inducing ligand (TRAIL)-induced apoptosis of melanoma cells. J Immunol *166*, 5337-5345.
Jeschke, J., Bizet, M., Desmedt, C., Calonne, E., Dedeurwaerder, S., Garaud, S., Koch, A., Larsimont, D., Salgado, R., Van den Eynden, G.*, et al.* (2017). DNA methylation-based immune response signature improves patient diagnosis in multiple cancers. J Clin Invest *127*, 3090-3102.
Kim, D., Pertea, G., Trapnell, C., Pimentel, H., Kelley, R., and Salzberg, S.L. (2013). TopHat2: accurate alignment of transcriptomes in the presence of insertions, deletions and gene fusions. Genome Biol *14*, R36.
Krueger, F., and Andrews, S.R. (2011). Bismark: a flexible aligner and methylation caller for Bisulfite-Seq applications. Bioinformatics *27*, 1571-1572.
Lai, F., Jiang, C.C., Farrelly, M.L., Zhang, X.D., and Hersey, P. (2012). Evidence for upregulation of Bim and the splicing factor SRp55 in melanoma cells from patients treated with selective BRAF inhibitors. Melanoma Res *22*, 244-251.
Leichter, A.L., Purcell, R.V., Sullivan, M.J., Eccles, M.R., and Chatterjee, A. (2015). Multi-platform microRNA profiling of hepatoblastoma patients using formalin fixed paraffin embedded archival samples. Gigascience *4*, 54.
Medvedeva, Y.A., Lennartsson, A., Ehsani, R., Kulakovskiy, I.V., Vorontsov, I.E., Panahandeh, P., Khimulya, G., Kasukawa, T., Consortium, F., and Drablos, F. (2015). EpiFactors: a comprehensive database of human epigenetic factors and complexes. Database (Oxford) *2015*, bav067.
Newman, A.M., Liu, C.L., Green, M.R., Gentles, A.J., Feng, W., Xu, Y., Hoang, C.D., Diehn, M., and Alizadeh, A.A. (2015). Robust enumeration of cell subsets from tissue expression profiles. Nat Methods *12*, 453-457.
Roberts, A., Trapnell, C., Donaghey, J., Rinn, J.L., and Pachter, L. (2011). Improving RNA-Seq expression estimates by correcting for fragment bias. Genome Biol *12*, R22.
Samur, M.K. (2014). RTCGAToolbox: a new tool for exporting TCGA Firehose data. PLoS One *9*, e106397.
Stockwell, P.A., Chatterjee, A., Rodger, E.J., and Morison, I.M. (2014). DMAP: differential methylation analysis package for RRBS and WGBS data. Bioinformatics *30*, 1814-1822.
Trapnell, C., Roberts, A., Goff, L., Pertea, G., Kim, D., Kelley, D.R., Pimentel, H., Salzberg, S.L., Rinn, J.L., and Pachter, L. (2012). Differential gene and transcript expression analysis of RNA-seq experiments with TopHat and Cufflinks. Nat Protoc *7*, 562-578.